(Preprint) AAS 24-144

EVALUATING DELTA-V DISPERSIONS USING LINEAR COVARIANCE TECHNIQUES WITH APPLICATIONS TO RENDEZVOUS AND DOCKING

David Woffinden*

One of the attractive advantages of using linear covariance analysis (LinCov) is that it can accurately produce both navigation errors and trajectory dispersions in a fraction of the time comparable to the standard Monte Carlo analysis approach that is traditionally adopted. It also has the capability of generating delta-v dispersions which is perhaps the most influential performance metric since many aspects of a mission design revolve around the anticipated propellant usage. Accurately capturing this key performance criteria using linear covariance techniques has several subtle caveats raising reasonable doubts and a cautious sense of skepticism. This paper outlines multiple approaches of modeling delta-v usage in LinCov, highlights their limitations and advantages, and ultimately compares their corresponding results to the *actual* Monte Carlo performance. The theory is also extended to reliably account for an arbitrary thruster configuration and the resultant propellant consumptions due to both translational burns and attitude maneuvers. This provides near instant insight into the impacts of thruster layout design and different vehicle mass properties. These derived techniques are applied and verified using an NRHO rendezvous and docking scenario consistent with upcoming NASA Artemis missions for Orion.

INTRODUCTION

It can be argued that the currency of spaceflight is delta-v or the amount of propellant required to complete a successful mission. Whether the phase of flight is rendezvous and docking, powered ascent, powered descent and landing, cis-lunar transfer, or on-orbit operations, the required velocity change to perform all the necessary translational and rotational burns is a key performance metric. For both mission success, crew safety, and operational feasibility, understanding the anticipated propellant usage becomes a critical aspect of the mission design and analysis. Accurately capturing this essential performance criteria becomes a challenging task, particularly in the presence of system uncertainty such as initial condition dispersions, navigation errors, disturbance acceleration and torques, maneuver execution errors, and other environmental impacts.

The standard approach traditionally adopted to derive the anticipated propellant usage is Monte Carlo analysis. An attractive alternate option is using linear covariance analysis (LinCov). In addition to reliably producing both navigation errors and trajectory dispersions, LinCov has the capability of generating the nominal delta-v and the expected delta-v dispersions in the fraction of the time compared to a Monte Carlo approach. Using linear covariance techniques for calculating this influential performance metric has several subtle caveats raising reasonable doubts and a cautious sense of skepticism.

This paper outlines multiple approaches of modeling delta-v usage in LinCov, highlights their limitations and advantages, and ultimately compares their corresponding results to the *actual* Monte Carlo performance. The theory is also extended to reliably account for an arbitrary thruster configuration and the resultant propellant consumptions due to both translational burns and attitude maneuvers. This provides near instant insight into the impacts of thruster layout design and different vehicle mass properties. These derived techniques are

*GN&C Autonomous Flight Systems Engineer, NASA JSC, Aeroscience and Flight Mechanics Division, david.c.woffinden@nasa.gov

applied and verified using an NRHO rendezvous and docking scenario consistent with the upcoming NASA Artemis missions for Orion.

DELTA-V AND PROPELLANT

When designing a trajectory to achieve the assortment of mission objectives, the resulting *delta-v* from the translational burns that alter the vehicle's velocity is directly connected to the total propellant required by the spacecraft thrusters to generate the necessary accelerations. The formal mathematical expression that connects delta-v to propellant usage is the infamous *rocket equation* credited to Konstantin Tsiolkovsky [1]. Consequently, it is not uncommon that the terms *delta-v* and *propellant* are used interchangeably in spaceflight. To some, they are synonymous.

In order to formally develop the linear covariance techniques for computing the delta-v and their dispersions for both impulsive and finite burns, the rocket equation is utilized [2]. A brief overview is provided now and referenced in later sections. According to the rocket equation, the magnitude of the velocity change that a propulsion system can produce $|\Delta\mathbf{v}|$ is a function of the initial mass m_i, the total expelled propellant mass prior to the impulsive maneuver m_e, the instantaneous change in mass expelled from the thruster Δm_e, the thrusters specific impulse I_{sp} in dimensions of time, and standard gravity g_0.

$$|\Delta\mathbf{v}| = (I_{sp} \cdot g) \ln \left[\frac{(m_i - m_e)}{(m_i - m_e) - \Delta m_e} \right] \tag{1}$$

The actual propellant mass expelled by the thruster to perform the specified impulsive burn can be determined by re-arranging Eqn 1 above.

$$\Delta m_e = (m_i - m_e) \left[1 - e^{-(\frac{|\Delta\mathbf{v}|}{I_{sp} \cdot g_0})} \right] \tag{2}$$

This formulation for the expelled mass for an impulsive burn can also be derived for a finite burn scenario when continuous thrust is assumed over a specified time interval. The amount of force applied by a thruster to a spacecraft is dependent on the expulsion of gases.

$$\mathbf{F} = \dot{m}_e \mathbf{v}_e + A_e \left[P_e - P_\infty \right] \approx \dot{m}_e \mathbf{v}_e \tag{3}$$

where A_e is the nozzle exit area, P_e is the gas pressure at nozzle exit, P_∞ is the ambient pressure (in space it is essentially zero), $\mathbf{v}_e$ is the propellant exhaust velocity, and $\dot{m}_e$ is the proplelant mass flow rate. The ratio of thrust to the weight flow rate of the propellant is the specific impulse, I_{sp}, which measures how efficient the propellant is converted into thrust.

$$I_{sp} = \frac{|\mathbf{F}|}{\dot{m}_e \cdot g_0} \tag{4}$$

such that the propellant exhaust velocity can be expressed as

$$|\mathbf{v}_e| = I_{sp} \cdot g_0 \tag{5}$$

Notice from Eq 3 that the mass flow rate is simply the ratio of the thruster force divided by the propellant exhaust velocity.

$$\dot{m}_e \approx \frac{|\mathbf{F}|}{|\mathbf{v}_e|} \tag{6}$$

Substituting the value for the exhaust velocity from Eqn 5 gives us the equation of motion governing the amount of mass expelled from the thruster given the I_{sp} of the thruster and standard gravity, g_0.

$$\dot{m}_e \approx \frac{|\mathbf{F}|}{I_{sp} \cdot g_0} \tag{7}$$

The force exerted on the spacecraft by a single thruster is equivalent to the current mass of the spacecraft times the acceleration the thruster produced. This can be expressed in terms of the initial mass, m_i, and the expelled mass, m_e.

$$\dot{m}_e \approx \left[\frac{(m_i - m_e)}{I_{sp} \cdot g_0} \right] |\mathbf{a}| \tag{8}$$

DELTA-V DISPERSIONS ANALYSIS APPROACH

To develop the different techniques to compute delta-v dispersions using linear covariance analysis, there are several performance metrics that must be defined which include the true trajectory dispersions $\delta\mathbf{x}$, the navigation dispersions $\delta\hat{\mathbf{x}}$, the true navigation error $\delta\mathbf{e}$, and the onboard navigation error $\delta\hat{\mathbf{e}}$ as depicted in Figure 1. The true dispersions $\delta\mathbf{x}$ are defined as the difference between the true state $\mathbf{x}$ and the nominal state

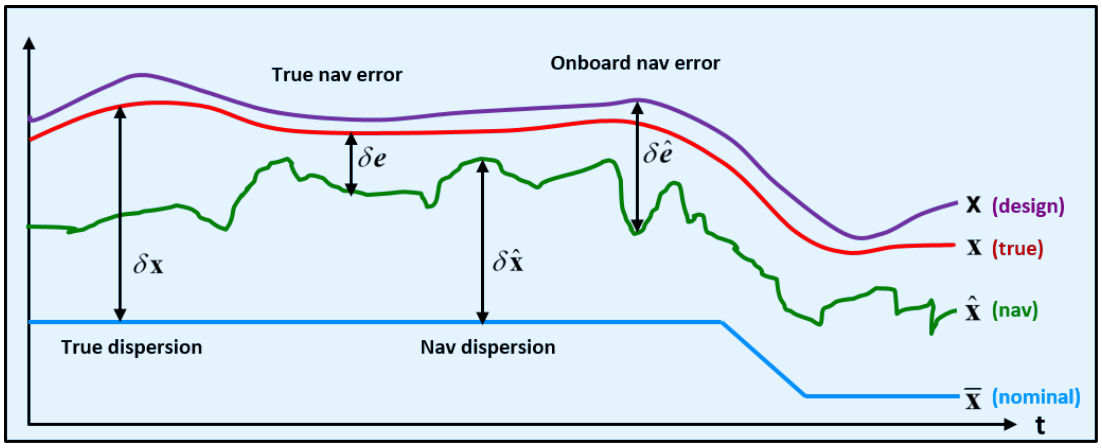


Figure 1. GN&C Performance Metric Variables

$\bar{\mathbf{x}}$. The true state $\mathbf{x}$ is an n-dimensional vector that represents the *real world* environment or actual state.

$$\delta\mathbf{x} \triangleq \mathbf{x} - \bar{\mathbf{x}} \qquad\qquad \mathbf{D} = E\left[\delta\mathbf{x}\delta\mathbf{x}^{\mathrm{T}}\right] \tag{9}$$

The nominal state $\bar{\mathbf{x}}$ is also an n-dimensional vector that represents the desired or reference state. The covariance of the environment dispersions, $\mathbf{D}$, indicates how precisely the system can follow a desired trajectory.

The navigation dispersions $\delta\hat{\mathbf{x}}$ are defined as the difference between the navigation state $\hat{\mathbf{x}}$ and the nominal state $\bar{\mathbf{x}}$. The navigation state is an $\hat{n}$-dimensional vector ($\hat{n} < n$) that represents the filter's estimated state.

$$\delta\hat{\mathbf{x}} \triangleq \hat{\mathbf{x}} - \mathbf{M}_x\bar{\mathbf{x}} \qquad\qquad \hat{\mathbf{D}} = E\left[\delta\hat{\mathbf{x}}\delta\hat{\mathbf{x}}^{\mathrm{T}}\right] \tag{10}$$

The matrix $\mathbf{M}_x$ is an $(\hat{n} \times n)$ matrix that maps the estimated state in terms of the true and nominal state. The covariance of the navigation dispersions, $\hat{\mathbf{D}}$, reflect how precisely the onboard system thinks it can follow a prescribed reference trajectory.

The true navigation error $\delta\mathbf{e}$ is the difference between the environment and navigation states. It is also the difference between the environment and the navigation dispersions.

$$\delta\mathbf{e} \triangleq \mathbf{M}_x\mathbf{x} - \hat{\mathbf{x}} = \mathbf{M}_x\delta\mathbf{x} - \delta\hat{\mathbf{x}} \qquad\qquad \mathbf{P} = E\left[\delta\mathbf{e}\delta\mathbf{e}^{\mathrm{T}}\right] \tag{11}$$

The covariance of the true navigation error, $\mathbf{P}$, quantifies how precisely the onboard navigation system can estimate the actual state.

The onboard navigation error $\delta\hat{\mathbf{e}}$ itself is never computed, but it is used to develop the onboard navigation filter equations. It is defined as the difference between the design state, x, and the navigation state $\hat{\mathbf{x}}$.

$$\delta\hat{\mathbf{e}} \triangleq \mathrm{x} - \hat{\mathbf{x}} \qquad\qquad \hat{\mathbf{P}} = E\left[\delta\hat{\mathbf{e}}\delta\hat{\mathbf{e}}^{\mathrm{T}}\right] \tag{12}$$

The covariance of the onboard navigation error, $\hat{\mathbf{P}}$, quantifies how precisely the onboard navigation system expects it can determine the actual state. The performance of the onboard navigation system is determined

by comparing $\hat{\mathbf{P}}$ to the actual navigation performance $\mathbf{P}$. If the *true* states and the *design* states are assumed to be the same, then the true navigation covariance will equal the onboard navigation covariance.

The covariances of the true dispersions, navigation dispersions, true navigation error, and the onboard navigation error are ultimately used to analyze and assess the performance of a proposed GN&C system. A common approach to obtain these performance metrics is to use a Monte Carlo simulation outlined in Figure 2, where the sample statistics of hundreds or thousands of runs, N, are used to numerically compute the desired covariance matrices.

$$\mathbf{D} = \frac{1}{N-1}\sum \delta\mathbf{x}\delta\mathbf{x}^{\mathrm{T}} \qquad \hat{\mathbf{D}} = \frac{1}{N-1}\sum \delta\hat{\mathbf{x}}\delta\hat{\mathbf{x}}^{\mathrm{T}} \qquad \mathbf{P} = \frac{1}{N-1}\sum \delta\mathbf{e}\delta\mathbf{e}^{\mathrm{T}} \tag{13}$$

The onboard navigation error covariance $\hat{\mathbf{P}}$ is the navigation filter covariance for each run. This same statistical information can be obtained using linear covariance analysis techniques.

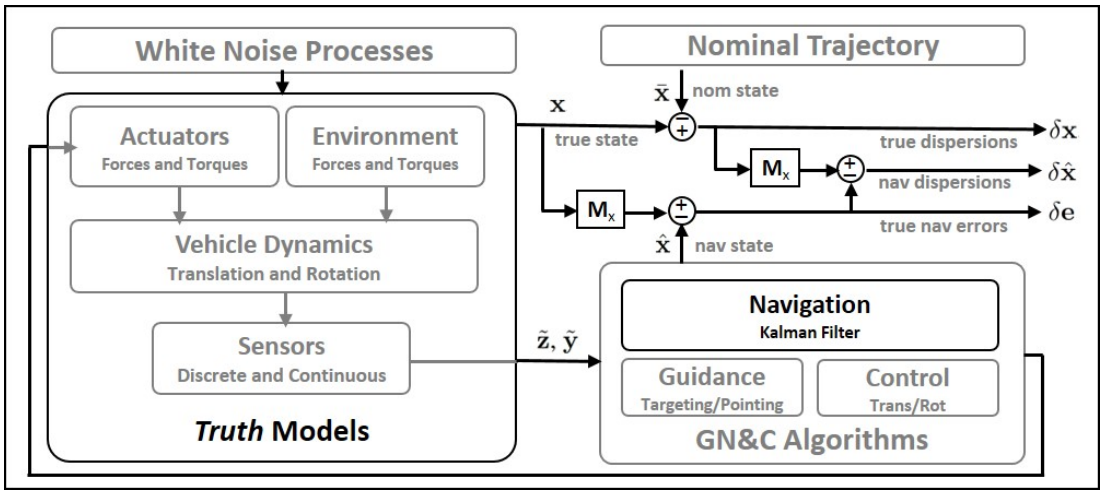


Figure 2. Extracting GN&C Performance Metrics Using Monte Carlo Techniques

Linear covariance analysis incorporates the non-linear system dynamics models and GN&C algorithms to generate a nominal reference trajectory $\bar{\mathbf{x}}$ which is then used to propagate, update, and correct an onboard navigation covariance matrix $\hat{\mathbf{P}}$ and an augmented state covariance matrix $\mathbf{C}$,

$$\mathbf{C} = E\left[\delta\mathbf{X}\delta\mathbf{X}^{\mathrm{T}}\right] \tag{14}$$

where the augmented state $\delta\mathbf{X}^{\mathrm{T}} = [\delta\mathbf{x}^{\mathrm{T}}\ \delta\hat{\mathbf{x}}^{\mathrm{T}}]$ consists of the true dispersions and the navigation dispersions. Pre- and post-multiplying the augmented state covariance matrix by the following mapping matrices, the covariances for the trajectory dispersions, navigation dispersions, and the navigation error can be obtained.

$$\begin{aligned}
\mathbf{D} &= [\,\mathbf{I}_{n\times n},\ \mathbf{0}_{n\times\hat{n}}\,]\,\mathbf{C}\,[\,\mathbf{I}_{n\times n},\ \mathbf{0}_{n\times\hat{n}}\,]^{\mathrm{T}} \\
\hat{\mathbf{D}} &= [\,\mathbf{0}_{\hat{n}\times n},\ \mathbf{I}_{\hat{n}\times\hat{n}}\,]\,\mathbf{C}\,[\,\mathbf{0}_{\hat{n}\times n},\ \mathbf{I}_{\hat{n}\times\hat{n}}\,]^{\mathrm{T}} \\
\mathbf{P} &= [\,\mathbf{I}_{\hat{n}\times n},\ -\mathbf{I}_{\hat{n}\times\hat{n}}\,]\,\mathbf{C}\,[\,\mathbf{I}_{\hat{n}\times n},\ -\mathbf{I}_{\hat{n}\times\hat{n}}\,]^{\mathrm{T}}
\end{aligned} \tag{15}$$

The linear covariance analysis equations used to propagate, update, and correct both the augmented state covariance matrix and the onboard navigation covariance matrix are summarized here along with the LinCov analysis inputs. For additional details regarding the development and implementation of the linear covariance simulation, see the following references [3–8].

Propagate The continuous-time propagation equations for the augmented state covariance matrix $\mathbf{C}$ and the onboard navigation covariance matrix $\hat{\mathbf{P}}$ are,

$$\dot{\mathbf{C}} = \mathbf{F}\mathbf{C} + \mathbf{C}\mathbf{F}^T + \mathbf{W}\mathbf{S}_w\mathbf{W}^T + \mathbf{V}\mathbf{S}_\nu\mathbf{V}^T + \mathbf{U}\mathbf{S}_\eta\mathbf{U}^T \tag{16}$$

$$\dot{\hat{\mathbf{P}}} = \hat{\mathbf{F}}\hat{\mathbf{P}} + \hat{\mathbf{P}}\hat{\mathbf{F}}^T + \hat{\mathbf{F}}_{\hat{w}}\hat{\mathbf{S}}_w\hat{\mathbf{F}}_{\hat{w}}^T + \left(\hat{\mathbf{F}}_{y_a}\hat{\mathbf{C}}^a_{\eta_a} + \hat{\mathbf{F}}_{y_\omega}\hat{\mathbf{C}}^\omega_{\eta_\omega}\right)\hat{\mathbf{S}}_\eta\left(\hat{\mathbf{F}}_{y_a}\hat{\mathbf{C}}^a_{\eta_a} + \hat{\mathbf{F}}_{y_\omega}\hat{\mathbf{C}}^\omega_{\eta_\omega}\right)^T \tag{17}$$

where $\mathbf{F}$ and $\hat{\mathbf{F}}$ are the augmented and onboard state dynamic Jacobians for the linearized perturbations dynamics about the reference trajectory. The mapping matrices $\mathbf{W}$, $\mathbf{V}$, and $\mathbf{U}$, are used to map the true dynamic, actuator, and continuous measurement process noise covariances, $\mathbf{S}_w$, $\mathbf{S}_\eta$, and $\mathbf{S}_\nu$ respectively, into $\mathbf{C}$. The navigation mapping matrices $\hat{\mathbf{F}}_{\hat{w}}$, $\hat{\mathbf{F}}_{y_a}$, $\hat{\mathbf{F}}_{y_\omega}$, $\hat{\mathbf{C}}^a_{\eta_a}$, and $\hat{\mathbf{C}}^\omega_{\eta_\omega}$ map the onboard dynamic and continuous accelerometer and gyro measurement process noise $\hat{\mathbf{S}}_w$ and $\hat{\mathbf{S}}_\eta$, into $\hat{\mathbf{P}}$.

Update The measurement update equations for augmented and navigation state covariance matrices, $\mathbf{C}$ and $\hat{\mathbf{P}}$, at a discrete measurement time are

$$\mathbf{C}^+ = \mathbf{H}\mathbf{C}^-\mathbf{H}^T + \mathbf{K}\mathbf{R}\mathbf{K}^T \tag{18}$$

$$\hat{\mathbf{P}}^+ = \left[\mathbf{I} - \hat{\mathbf{K}}\hat{\mathbf{H}}\right]\hat{\mathbf{P}}^-\left[\mathbf{I} - \hat{\mathbf{K}}\hat{\mathbf{H}}\right]^T + \hat{\mathbf{K}}\hat{\mathbf{R}}\hat{\mathbf{K}}^T \tag{19}$$

where $\mathbf{C}^+$ and $\hat{\mathbf{P}}^+$ represent the updated augmented and navigation covariance matrices and $\hat{\mathbf{K}}$ is the Kalman gain.

$$\hat{\mathbf{K}} = \hat{\mathbf{P}}^-\hat{\mathbf{H}}^T\left[\hat{\mathbf{H}}\hat{\mathbf{P}}^-\hat{\mathbf{H}}^T + \hat{\mathbf{R}}\right]^{-1} \tag{20}$$

The matrices $\hat{\mathbf{H}}$ and $\hat{\mathbf{R}}$ are the measurement sensitivity and measurement noise matrices respectively. The matrices $\mathbf{H}$ and $\mathbf{K}$ map the effects of the measurements and their associated noise to the navigation state dispersions.

Correct The correction equations for impulsive translational burns for the augmented state and onboard state covariances, $\mathbf{C}$ and $\hat{\mathbf{P}}$, at the nominal maneuver time are

$$\mathbf{C}^+ = \mathbf{G}\mathbf{C}^-\mathbf{G}^T + \mathbf{N}\boldsymbol{S}_w\mathbf{N}^T \tag{21}$$

$$\hat{\mathbf{P}}^+ = \left[\hat{\mathbf{I}} + \hat{\mathbf{G}}\right]\hat{\mathbf{P}}^-\left[I + \hat{\mathbf{G}}\right]^T + \hat{\mathbf{N}}\hat{\mathbf{S}}_w\hat{\mathbf{N}}^T \tag{22}$$

The matrices $\mathbf{G}$ and $\hat{\mathbf{G}}$ contain the control partials associated with a linearized rendezvous targeting algorithms. The matrices $\mathbf{N}$ and $\hat{\mathbf{N}}$ are used to map the effects of actuator noise, described by $\boldsymbol{S}_w$ and $\hat{\mathbf{S}}^w$, into $\mathbf{C}$ and $\hat{\mathbf{P}}$.

THRUSTER MODELING

For mission design and analysis a common actuator or thruster model used to capture the impacts of doing impulsive translational burns is the Gate's model [9], which was originally intended to model the errors associated with trajectory midcourse correction maneuvers during the ballistic lunar and interplanetary flight phases. The resulting execution error model accounted for four independent error sources including a *shutoff*, *resolution*, *pointing*, and *autopilot* errors. The executed delta-v in the inertial frame $\Delta\mathbf{v}^i$ that accounts for these error sources is expressed mathematically as

$$\Delta\mathbf{v}^i = \mathbf{T}^i_b\mathbf{T}^b_a\left[\left(\mathbf{I} - [\boldsymbol{\epsilon}^a_{\Delta v}\times] + \mathbf{I}s_{\Delta v}\right)\Delta\check{\mathbf{v}}^a + \mathbf{b}^a_{\Delta v}\right] \tag{23}$$

where the error parameters are expressed in the thruster actuator frame and ultimately transformed to the inertial frame using the thruster actuator-to-body $\mathbf{T}^b_a$ and body-to-inertial $\mathbf{T}^i_b$ transformation matrices. The

shutoff error $s_{\Delta v}$ is modeled as a scale-factor in the shutoff system or a proportional magnitude error, $\boldsymbol{\epsilon}^a_{\Delta v}$ represents the *pointing* error or the error in the angular orientation of the thrust vector such as a proportional pointing or misalignment error, $\mathbf{b}^a_{\Delta v}$ consists of the *resolution* error (b_x) or the error in computation and transmission (fixed magnitude error) and *autopilot* error (b_y and b_z) which is due to the behavior of the autopilot control system (fixed pointing error).

$$\mathbf{b}^a_{\Delta v} = [b_x, b_y, b_z]^T \tag{24}$$

As depicted in Figure 3, when only a single thruster is assumed, the actuator is aligned with the commanded delta-v such that the command delta-v is along the thruster x-axis, $\Delta\check{\mathbf{v}}^a = [\Delta\check{v}, 0, 0]^T$.

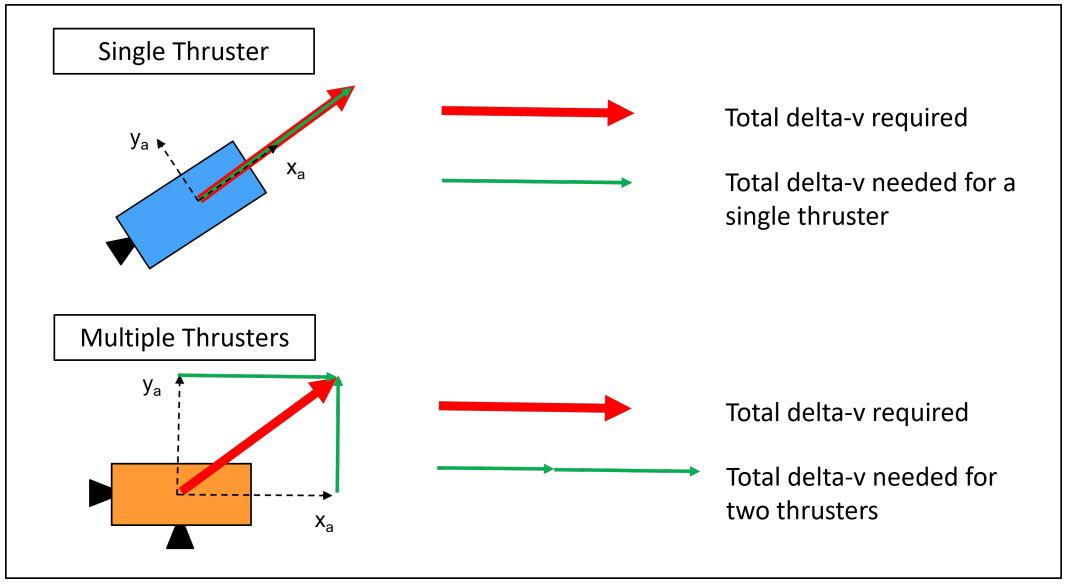


Figure 3. Thruster Configuration Options

The Gate's model does not explicitly include attitude errors so effects of the vehicle's attitude determination and control system with star trackers or gyros are not directly modeled. The Gate's model *pointing* error term, $\boldsymbol{\epsilon}^t_t$, attempts to account for both the pointing knowledge error (navigation) and actuator misalignment (structural/control) into one. For small trajectory correction burns, this is reasonable but for larger non-zero rendezvous burns this is a noticeable limitation. Additionally, the Gate's model does not include persistent error sources which is an appropriate assumption for interplanetary travel when the time interval between correction burns can be on the order of multiple days or weeks and there are little to no correlation in the execution errors from one burn to the next. For rendezvous and docking scenarios where subsequent burns can be on the order of seconds to minutes this correlation is more pertinent. In addition, for rendezvous the burns are typically non-zero such that capturing the impacts of the vehicle's attitude determination system is more critical. Consequently, the assumptions underlying the Gate's model begin to break down for scenarios like rendezvous and docking.

Geller introduce a more general model [4] that addresses these short comings for linear covariance analysis. The updated thruster model includes the vehicle's attitude errors $\boldsymbol{\theta}^b$ and models the thruster error parameters as exponentially correlated random variables such that the errors can be correlated in time such as the thruster misalignment $\boldsymbol{\epsilon}^t_t$ and bias $\mathbf{b}^t_t$. Thruster noise is also included $\boldsymbol{\nu}^t_t$.

$$\Delta\mathbf{v}^i = \bar{\mathbf{T}}^i_b \left(\mathbf{I} + [\boldsymbol{\theta}^b\times]\right) \bar{\mathbf{T}}^b_a \left[\left(\mathbf{I} - [\boldsymbol{\epsilon}^a_{\Delta v}\times] + \mathbf{I}s_{\Delta v}\right) \Delta\check{\mathbf{v}}^a + \mathbf{b}^a_{\Delta v} + \boldsymbol{\nu}^a_{\Delta v}\right] \tag{25}$$

This higher fidelity model of the burn execution errors essentially extends the Gate's model and captures the impacts of the vehicle's attitude determination and control system with error parameters that can be time-correlated by using exponentially correlated random variables (ECRV).

Up to this point, the thruster models have assumed either the vehicle orients itself to align a single thruster with the commanded delta-v or the actuator system can be characterized as a single thruster in executing the required velocity change. In terms of impacts on the vehicle's trajectory and motion, these assumptions are reasonable. However, if the intent is to extract the spaceflight currency of propellant usage, these assumptions mask additional *delta-v* truly required to complete the mission successfully. This concept is illustrated in Figure 3 where the required delta-v is depicted with the red arrow. For a single thruster that is aligned with the commanded delta-v, the total delta-v from the only thruster is the same (as emphasized with the green arrow). However, if the required delta-v needs to be generated with multiple thrusters in a fixed configuration with an arbitrary vehicle orientation where the thrusters are not necessarily aligned with the commanded delta-v, now the sum total delta-v needed for a multiple thruster system (two green arrows) is greater than the magnitude of the commanded delta-v (single red arrow).

Extending this perspective, if multiple thrusters serve a dual purpose as both translational and rotational actuators, the total delta-v (or propellant usage) to perform both functions also increases. Including the potential of cross-coupling between both, not only is propellant consumption impacted but also the vehicle rotational and translational dynamics. Lastly, what if the burns are not adequately modeled as impulsive burns but need to be captured as finite burns? Is there a thruster actuator model that captures these effects and how can it be implemented in a linear covariance simulation tool?

A general thruster layout configuration for the vehicle's actuators and its impact on both the propellant calculation and the vehicle rotational and translational dynamics is captured in Figure 4 for both an *open-loop* and *closed-loop* GN&C system architecture. This figure summarizes the complex interaction between the system dynamics, navigation sensor suite, the GN&C flight software algorithms, and the vehicle's actuators to achieve a desired trajectory profile. The true vehicle states $\mathbf{x}$ drive both discrete $\tilde{\mathbf{z}}$ and continuous $\tilde{\mathbf{y}}$ sensor measurements. These sensor measurements are then processed by an onboard navigation system that estimates the vehicle's state $\hat{\mathbf{x}}$ in order to properly guide and control the spacecraft. Given an estimate of the vehicle's state, the guidance system determines the desired reference trajectory $\bar{\mathbf{r}}$ for the vehicle to follow which serves as an input to the vehicle's control system that computes a commanded input $\hat{\mathbf{u}}$ to activate the available actuators. The actuators impart various forces, torques, or impulsive velocity changes $\mathbf{u}$ which in turn alters the vehicle dynamics and this closed-loop process is repeated until the final destination or objective is achieved.

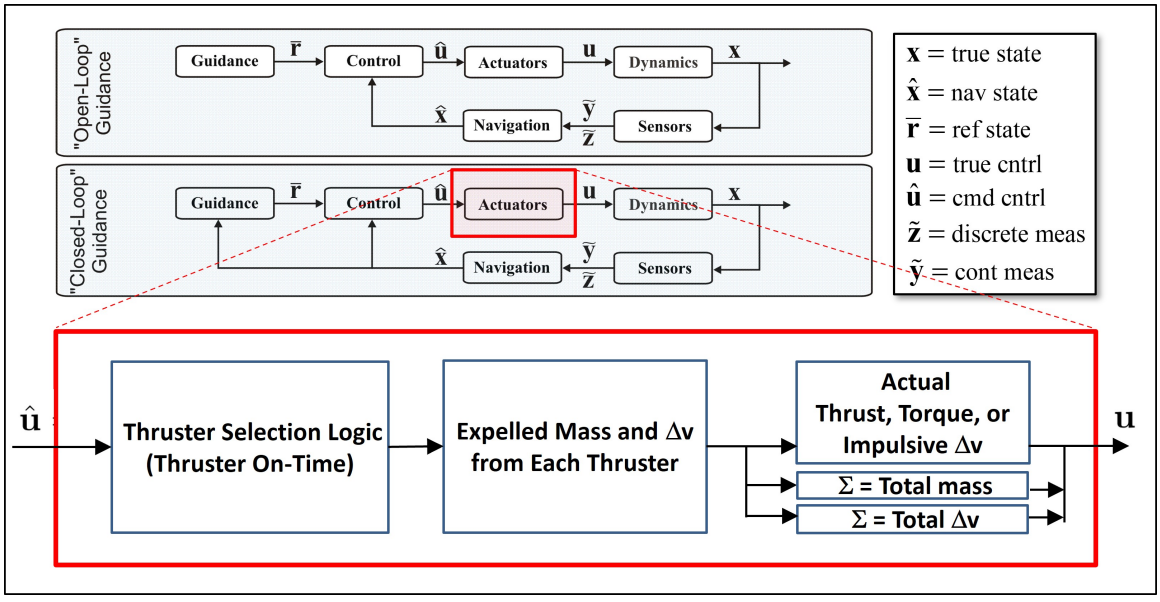


Figure 4. Open-Loop and Closed-Loop Thruster Configurations

The lower half of Figure 4 exposes details of the vehicle's actuator system that receives commanded forces, torques, or impulsive velocity changes $\hat{\mathbf{u}}$ and then determines which thruster's to activate and the burn duration to achieve the required velocity or angular rate change. The propellant expelled mass and delta-v from each thruster is then used to determine 1) the impacts on the actual forces, torques, or impulsive velocity changes $\mathbf{u}$ imparted on the spacecraft, and 2) the resultant total propellant and total delta-v utilized. The remainder of the paper will focus on how to determine in a linear covariance framework the total propellant and total delta-v required for 1) single and multiple thruster configurations, 2) impulsive delta-v and finite thruster burns and 3) using jets for both translational and rotational control.

NRHO RPOD LINCOV MODELS

To motivate the linear covariance equations and implementation of the total propellant or delta-v required for the different thruster models, the equations are developed in context of a rendezvous and docking problem between an active chaser vehicle and a passive target vehicle in a near rectilinear halo orbit (NRHO). For linear covariance analysis, it is important to define the *true* and the *navigation* states and their corresponding dynamics in order to derive the expressions to propagate the augmented state covariance matrix $\mathbf{C}$. To develop the equations of motion for the onboard or filter state covariance matrix $\hat{\mathbf{P}}$, the *design* states are utilized.

NRHO RPOD States

The true states $\mathbf{x}$ for the rendezvous and docking problem consist of the chaser vehicle states $\mathbf{x}_c$, target vehicle states $\mathbf{x}_t$, inertial measurement parameter states $\mathbf{x}_{\tilde{y}}$, actuator states $\mathbf{x}_u$, and performance states $\mathbf{x}_p$.

$$\mathbf{x} = [\mathbf{x}_c;\ \mathbf{x}_t;\ \mathbf{x}_{\tilde{y}};\ \mathbf{x}_u;\ \mathbf{x}_p] \tag{26}$$

The four vehicle state vectors include the Moon-centered inertial position $\mathbf{r}_c^i$, inertial velocity $\mathbf{v}_c^i$, inertial-to-body quaternion $\mathbf{q}_i^c$, and the body angular rates in body coordinates $\boldsymbol{\omega}_c^c$.

$$\mathbf{x}_c = [\mathbf{r}_c^i;\ \mathbf{v}_c^i;\ \mathbf{q}_i^c;\ \boldsymbol{\omega}_c^c] \tag{27}$$

Similarly, the four target vehicle states are comprised of the Moon-centered inertial position $\mathbf{r}_t^i$, inertial velocity $\mathbf{v}_t^i$, inertial-to-body quaternion $\mathbf{q}_i^t$, and the body angular rates in body coordinates $\boldsymbol{\omega}_t^t$.

$$\mathbf{x}_t = [\mathbf{r}_t^i;\ \mathbf{v}_t^i;\ \mathbf{q}_i^t;\ \boldsymbol{\omega}_t^t] \tag{28}$$

There are 6 inertial sensor parameter states including the accelerometer bias $\mathbf{b}_{\tilde{a}}$, accelerometer scale factor $\mathbf{s}_{\tilde{a}}$, accelerometer misalignment $\boldsymbol{\epsilon}_{\tilde{a}}$, gyro bias $\mathbf{b}_{\tilde{\omega}}$, gyro scale factor $\mathbf{s}_{\tilde{\omega}}$, and gyro misalignment $\boldsymbol{\epsilon}_{\tilde{\omega}}$.

$$\mathbf{x}_{\tilde{y}} = [\mathbf{b}_{\tilde{a}}^c;\ \mathbf{s}_{\tilde{a}}^c;\ \boldsymbol{\epsilon}_{\tilde{a}}^c;\ \mathbf{b}_{\tilde{\omega}}^c;\ \mathbf{s}_{\tilde{\omega}}^c;\ \boldsymbol{\epsilon}_{\tilde{\omega}}^c] \tag{29}$$

The actuator parameter states also have 6 states which are the thrust actuator bias $\mathbf{b}_{_T}^a$, thrust actuator scale factor $\mathbf{s}_{_T}^a$, thrust actuator misalignment $\boldsymbol{\epsilon}_{_T}^a$, torque actuator bias $\mathbf{b}_\tau^a$, torque actuator scale factor $\mathbf{s}_\tau^a$, and torque actuator misalignment $\boldsymbol{\epsilon}_\tau^a$;

$$\mathbf{x}_u = [\mathbf{b}_{_T}^a;\ \mathbf{s}_{_T}^a;\ \boldsymbol{\epsilon}_{_T}^a;\ \mathbf{b}_\tau^a;\ \mathbf{s}_\tau^a;\ \boldsymbol{\epsilon}_\tau^a] \tag{30}$$

Lastly, the performance parameter states consists of the total expelled propellant mass m_e, specific impulse of each thruster $\mathbf{b}_{Isp_k}$, and time t.

$$\mathbf{x}_p = [m_e;\ b_{Isp_1};\ \ b_{Isp_2};\ \ldots\ b_{Isp_n};\ \ t] \tag{31}$$

NRHO RPOD State Propagation

The true state dynamics are a function of the true states $\mathbf{x}$, the non-gravitational acceleration inputs $\mathbf{u}_a^i$, the non-gravitational torque inputs $\mathbf{u}_\tau^c$, and the system process noise $\mathbf{w}$.

$$\dot{\mathbf{x}} = \mathbf{f}(\mathbf{x}, \mathbf{u}_a^i, \mathbf{u}_\tau^c, \mathbf{w}) \tag{32}$$

True (Environment) States	Navigation States	Design States
Chaser Vehicle States, $\mathbf{x}_c$		
$\dot{\mathbf{r}}_c^i = \mathbf{v}_c^i$ $\dot{\mathbf{v}}_c^i = \mathbf{u}_a^i + \left(\mathbf{a}_{grv_c}^i + \mathbf{w}_{grv_c}^i\right)$ $\dot{\mathbf{q}}_i^c = \frac{1}{2}\boldsymbol{\omega}_c^c \otimes \mathbf{q}_i^c$ $\dot{\boldsymbol{\omega}}_c^c = {I_c}^{-1}\left[\mathbf{u}_\tau^c - \boldsymbol{\omega}_c^c \times I_c\, \boldsymbol{\omega}_c^c\right] + \mathbf{w}_\alpha^c$	$\dot{\hat{\mathbf{r}}}_c^i = \hat{\mathbf{v}}_c^i$ $\dot{\hat{\mathbf{v}}}_c^i = \check{\mathbf{y}}_{\tilde{\mathbf{a}}}^i + \hat{\mathbf{a}}_{grv_c}^i$ $\dot{\hat{\boldsymbol{\theta}}}_c^c = (\check{\mathbf{y}}_{\tilde{\boldsymbol{\omega}}}^c - \bar{\boldsymbol{\omega}}_c^c) - \bar{\boldsymbol{\omega}}_c^c \times \hat{\boldsymbol{\theta}}_c^c$	$\dot{\mathrm{r}}_c^i = \mathrm{v}_c^i$ $\dot{\mathrm{v}}_c^i = \mathrm{u}_a^i + \left(\mathrm{a}_{grv_c}^i + \hat{\mathbf{w}}_{grv_c}^i\right)$ $\dot{\mathrm{q}}_i^c = \frac{1}{2}\mathrm{w}_c^c \otimes \mathrm{q}_i^c$ $\dot{\mathrm{w}}_c^c = {\mathrm{I_c}}^{-1}\left[\mathrm{u}_\tau^c - \mathrm{w}_c^c \times \mathrm{I_c}\, \mathrm{w}_c^c\right] + \hat{\mathbf{w}}_\alpha^c$
Target Vehicle States, $\mathbf{x}_t$		
$\dot{\mathbf{r}}_t^i = \mathbf{v}_t^i$ $\dot{\mathbf{v}}_t^i = \mathbf{a}_{grv_t}^i + \mathbf{w}_{grv_t}^i$ $\dot{\mathbf{q}}_i^t = \frac{1}{2}\boldsymbol{\omega}_t^t \otimes \mathbf{q}_i^t$ $\dot{\boldsymbol{\omega}}_t^t = -{I_t}^{-1}\left[\boldsymbol{\omega}_t^t \times I_t\, \boldsymbol{\omega}_t^t\right] + \mathbf{w}_\alpha^t$	$\dot{\hat{\mathbf{r}}}_t^i = \hat{\mathbf{v}}_t^i$ $\dot{\hat{\mathbf{v}}}_t^i = \hat{\mathbf{a}}_{grv_t}^i$ $\dot{\hat{\boldsymbol{\theta}}}_t^t = \left(\boldsymbol{\omega}_t^t - \hat{\boldsymbol{\omega}}_t^t\right) - \hat{\boldsymbol{\omega}}_t^t \times \hat{\boldsymbol{\theta}}_t^t$	$\dot{\mathrm{r}}_t^i = \mathrm{v}_t^i$ $\dot{\mathrm{v}}_t^i = \mathrm{a}_{grv_t}^i + \hat{\mathbf{w}}_{grv_t}^i$ $\dot{\mathrm{q}}_i^t = \frac{1}{2}\mathrm{w}_t^t \otimes \mathrm{q}_i^t$ $\dot{\mathrm{w}}^t = -\mathrm{I}_t^{-1}\left[\mathrm{w}_t^t \times \mathrm{I_t}\, \mathrm{w}_t^t\right] + \hat{\mathbf{w}}_\alpha^t$
Inertial Sensor States, $\mathbf{x}_{\tilde{y}}$		
$\dot{\mathbf{b}}_{\tilde{a}}^b = -\mathbf{b}_{\tilde{a}}^b/\tau_{b_{\tilde{a}}} + \mathbf{w}_{b_{\tilde{a}}}^b$ $\dot{\mathbf{s}}_{\tilde{a}}^b = -\mathbf{s}_{\tilde{a}}^b/\tau_{s_{\tilde{a}}} + \mathbf{w}_{s_{\tilde{a}}}^b$ $\dot{\boldsymbol{\epsilon}}_{\tilde{a}}^b = -\boldsymbol{\epsilon}_{\tilde{a}}^b/\tau_{\epsilon_{\tilde{a}}} + \mathbf{w}_{\epsilon_{\tilde{a}}}^b$ $\dot{\mathbf{b}}_{\tilde{\omega}}^b = -\mathbf{b}_{\tilde{\omega}}^b/\tau_{b_{\tilde{\omega}}} + \mathbf{w}_{b_{\tilde{\omega}}}^b$ $\dot{\mathbf{s}}_{\tilde{\omega}}^b = -\mathbf{s}_{\tilde{\omega}}^b/\tau_{s_{\tilde{\omega}}} + \mathbf{w}_{s_{\tilde{\omega}}}^b$ $\dot{\boldsymbol{\epsilon}}_{\tilde{\omega}}^b = -\boldsymbol{\epsilon}_{\tilde{\omega}}^b/\tau_{\epsilon_{\tilde{\omega}}} + \mathbf{w}_{\epsilon_{\tilde{\omega}}}^b$	$\dot{\hat{\mathbf{b}}}_{\tilde{a}}^b = -\hat{\mathbf{b}}_{\tilde{a}}^b/\tau_{b_{\tilde{a}}}$ $\dot{\hat{\mathbf{s}}}_{\tilde{a}}^b = -\hat{\mathbf{s}}_{\tilde{a}}^b/\tau_{s_{\tilde{a}}}$ $\dot{\hat{\boldsymbol{\epsilon}}}_{\tilde{a}}^b = -\hat{\boldsymbol{\epsilon}}_{\tilde{a}}^b/\tau_{\epsilon_{\tilde{a}}}$ $\dot{\hat{\mathbf{b}}}_{\tilde{\omega}}^b = -\hat{\mathbf{b}}_{\tilde{\omega}}^b/\tau_{b_{\tilde{\omega}}}$ $\dot{\hat{\mathbf{s}}}_{\tilde{\omega}}^b = -\hat{\mathbf{s}}_{\tilde{\omega}}^b/\tau_{s_{\tilde{\omega}}}$ $\dot{\hat{\boldsymbol{\epsilon}}}_{\tilde{\omega}}^b = -\hat{\boldsymbol{\epsilon}}_{\tilde{\omega}}^b/\tau_{\epsilon_{\tilde{\omega}}}$	$\dot{\mathrm{b}}_{\tilde{a}}^b = -\mathrm{b}_{\tilde{a}}^b/\tau_{b_{\tilde{a}}} + \hat{\mathbf{w}}_{b_{\tilde{a}}}^b$ $\dot{\mathrm{s}}_{\tilde{a}}^b = -\mathrm{s}_{\tilde{a}}^b/\tau_{s_{\tilde{a}}} + \hat{\mathbf{w}}_{s_{\tilde{a}}}^b$ $\dot{\boldsymbol{\epsilon}}_{\tilde{a}}^b = -\boldsymbol{\epsilon}_{\tilde{a}}^b/\tau_{\epsilon_{\tilde{a}}} + \hat{\mathbf{w}}_{\epsilon_{\tilde{a}}}^b$ $\dot{\mathrm{b}}_{\tilde{\omega}}^b = -\mathrm{b}_{\tilde{\omega}}^b/\tau_{b_{\tilde{\omega}}} + \hat{\mathbf{w}}_{b_{\tilde{\omega}}}^b$ $\dot{\mathrm{s}}_{\tilde{\omega}}^b = -\mathrm{s}_{\tilde{\omega}}^b/\tau_{s_{\tilde{\omega}}} + \hat{\mathbf{w}}_{s_{\tilde{\omega}}}^b$ $\dot{\boldsymbol{\epsilon}}_{\tilde{\omega}}^b = -\boldsymbol{\epsilon}_{\tilde{\omega}}^b/\tau_{\epsilon_{\tilde{\omega}}} + \hat{\mathbf{w}}_{\epsilon_{\tilde{\omega}}}^b$
Actuator States, $\mathbf{x}_u$		
$\dot{\mathbf{b}}_T^a = -\mathbf{b}_T^a/\tau_{b_T} + \mathbf{w}_{b_T}^a$ $\dot{\mathbf{s}}_T^a = -\mathbf{s}_T^a/\tau_{s_T} + \mathbf{w}_{s_T}^a$ $\dot{\boldsymbol{\epsilon}}_T^a = -\boldsymbol{\epsilon}_T^a/\tau_{\epsilon_T} + \mathbf{w}_{\epsilon_T}^a$ $\dot{\mathbf{b}}_\tau^a = -\mathbf{b}_\tau^a/\tau_{b_\tau} + \mathbf{w}_{b_\tau}^a$ $\dot{\mathbf{s}}_\tau^a = -\mathbf{s}_\tau^a/\tau_{s_\tau} + \mathbf{w}_{s_\tau}^a$ $\dot{\boldsymbol{\epsilon}}_\tau^a = -\boldsymbol{\epsilon}_\tau^a/\tau_{\epsilon_\tau} + \mathbf{w}_{\epsilon_\tau}^a$	$\dot{\hat{\mathbf{b}}}_T^a = -\hat{\mathbf{b}}_T^a/\tau_{b_T}$ $\dot{\hat{\mathbf{s}}}_T^a = -\hat{\mathbf{s}}_T^a/\tau_{s_T}$ $\dot{\hat{\boldsymbol{\epsilon}}}_T^a = -\hat{\boldsymbol{\epsilon}}_T^a/\tau_{\epsilon_T}$ $\dot{\hat{\mathbf{b}}}_\tau^a = -\hat{\mathbf{b}}_\tau^a/\tau_{b_\tau}$ $\dot{\hat{\mathbf{s}}}_\tau^a = -\hat{\mathbf{s}}_\tau^a/\tau_{s_\tau}$ $\dot{\hat{\boldsymbol{\epsilon}}}_\tau^a = -\hat{\boldsymbol{\epsilon}}_\tau^a/\tau_{\epsilon_\tau}$	$\dot{\mathrm{b}}_T^a = -\mathrm{b}_T^a/\tau_{b_T} + \hat{\mathbf{w}}_{b_T}^a$ $\dot{\mathrm{s}}_T^a = -\mathrm{s}_T^a/\tau_{s_T} + \hat{\mathbf{w}}_{s_T}^a$ $\dot{\boldsymbol{\epsilon}}_T^a = -\boldsymbol{\epsilon}_T^a/\tau_{\epsilon_T} + \hat{\mathbf{w}}_{\epsilon_T}^a$ $\dot{\mathrm{b}}_\tau^a = -\mathrm{b}_\tau^a/\tau_{b_\tau} + \hat{\mathbf{w}}_{b_\tau}^a$ $\dot{\mathrm{s}}_\tau^a = -\mathrm{s}_\tau^a/\tau_{s_\tau} + \hat{\mathbf{w}}_{s_\tau}^a$ $\dot{\boldsymbol{\epsilon}}_\tau^a = -\boldsymbol{\epsilon}_\tau^a/\tau_{\epsilon_\tau} + \hat{\mathbf{w}}_{\epsilon_\tau}^a$
Performance States, $\mathbf{x}_p$		
$\dot{m}_e = \sum_{k=1}^{n} \beta_k$ $\dot{b}_{Isp_k} = -b_{Isp_k}/\tau_{b_{Isp_k}} + w_{b_{Isp_k}}$ $\dot{t} = 1$	$\dot{\hat{m}}_e = \sum_{k=1}^{n} \hat{\beta}_k$ $\dot{\hat{b}}_{Isp_k} = -\hat{b}_{Isp_k}/\tau_{b_{Isp_k}}$ $\dot{\hat{t}} = 1$	$\dot{\mathrm{m}}_e = \sum_{k=1}^{n} \beta_k$ $\dot{\mathrm{b}}_{Isp_k} = -\mathrm{b}_{Isp_k}/\tau_{b_{Isp_k}} + \hat{w}_{b_{Isp_k}}$ $\dot{\mathrm{t}} = 1$
$\dot{\mathbf{x}} = \mathbf{f}(\mathbf{x}, \mathbf{u}_a^i, \mathbf{u}_\tau^c, \mathbf{w})$	$\dot{\hat{\mathbf{x}}} = \hat{\mathbf{f}}(\hat{\mathbf{x}}, \check{\mathbf{y}}_{\tilde{\mathbf{a}}}^i, \check{\mathbf{y}}_{\tilde{\boldsymbol{\omega}}}^c)$	$\dot{\mathrm{x}} = \hat{\mathbf{f}}(\mathrm{x}, \mathrm{u}_a^i, \mathrm{u}_\tau^c, \hat{\mathbf{w}})$

Table 1. True and Navigation State Dynamics

The system process noise includes the gravitational, rotational, and parameter state noise terms, $\mathbf{w} = [\mathbf{w}_{grv}^i; \mathbf{w}_\alpha^c; \mathbf{w}_p]$, such that the covariance of the system process noise is given by

$$E[\mathbf{w}(t)\mathbf{w}(t)^T] = \mathbf{S}_w(t)\delta(t - t') \tag{33}$$

The navigation state dynamics incorporated the compensated accelerometer $\check{\mathbf{y}}_{\tilde{\mathbf{a}}}^i$ and gyro $\check{\mathbf{y}}_{\tilde{\boldsymbol{\omega}}}^c$ measurements to estimate both the translational and rotational dynamics.

$$\dot{\hat{\mathbf{x}}} = \hat{\mathbf{f}}(\hat{\mathbf{x}}, \check{\mathbf{y}}_{\tilde{\mathbf{a}}}^i, \check{\mathbf{y}}_{\tilde{\boldsymbol{\omega}}}^c) \tag{34}$$

The design state dynamics used to develop the onboard filter equations includes the design state x, the non-gravitational acceleration inputs, the non-gravitational torque inputs, and the tuned filter process noise $\hat{\mathbf{w}}$,

$$\dot{\mathrm{x}} = \hat{\mathbf{f}}(\mathrm{x}, \mathrm{u}_a^i, \mathrm{u}_\tau^c, \hat{\mathbf{w}}) \tag{35}$$

The filter process noise includes the gravitational, rotational, and parameter state noise terms, $\hat{\mathbf{w}} = [\hat{\mathbf{w}}_{grv}^i; \hat{\mathbf{w}}_\alpha^c; \hat{\mathbf{w}}_p]$, such that the covariance of the filter process noise is given by

$$E[\hat{\mathbf{w}}(t)\hat{\mathbf{w}}(t)^T] = \hat{\mathbf{S}}_w(t)\delta(t-t') \tag{36}$$

The true, navigation, and design state dynamics are summarized in Table 1.

Gravitational Forces and Torques For dynamics in a near rectilinear halo-orbit (NRHO), no gravitational torques are assumed for either vehicle but a multi-body gravity model for both the chaser and target spacecraft acceleration is utilized,

$$\mathbf{f}_{grv_c}^i = \mathbf{g}_{grv}(\mathbf{x}_c) = -(m_c)\mathbf{a}_{grv_c}^i = -(m_i - m_e)\mathbf{a}_{grv_c}^i \tag{37}$$

$$\mathbf{f}_{grv_t}^i = \mathbf{g}_{grv}(\mathbf{x}_t) = -(m_t)\mathbf{a}_{grv_t}^i \tag{38}$$

where m_c and m_t are the mass of the chaser and target vehicles respectively. The chaser's current mass equals its initial mass m_i minus the propellant expelled mass m_e. The gravitational acceleration assumes the Moon is the central body with the Earth and Sun as secondary celestial bodies such that

$$\mathbf{a}_{grv_c}^i = -\mu_{_M}\left(\frac{\mathbf{r}_c^i}{|\mathbf{r}_c^i|^3}\right) - \mu_{_E}\left(\frac{(\mathbf{r}_c^i - \mathbf{r}_{E/M}^i)}{|(\mathbf{r}_c^i - \mathbf{r}_{E/M}^i)|^3} + \frac{\mathbf{r}_{E/M}^i}{|\mathbf{r}_{E/M}^i|^3}\right) - \mu_{_S}\left(\frac{(\mathbf{r}_c^i - \mathbf{r}_{S/M}^i)}{|(\mathbf{r}_c^i - \mathbf{r}_{S/M}^i)|^3} + \frac{\mathbf{r}_{S/M}^i}{|\mathbf{r}_{S/M}^i|^3}\right) \tag{39}$$

$$\mathbf{a}_{grv_t}^i = -\mu_{_M}\left(\frac{\mathbf{r}_t^i}{|\mathbf{r}_t^i|^3}\right) - \mu_{_E}\left(\frac{(\mathbf{r}_t^i - \mathbf{r}_{E/M}^i)}{|(\mathbf{r}_t^i - \mathbf{r}_{E/M}^i)|^3} + \frac{\mathbf{r}_{E/M}^i}{|\mathbf{r}_{E/M}^i|^3}\right) - \mu_{_S}\left(\frac{(\mathbf{r}_t^i - \mathbf{r}_{S/M}^i)}{|(\mathbf{r}_t^i - \mathbf{r}_{S/M}^i)|^3} + \frac{\mathbf{r}_{S/M}^i}{|\mathbf{r}_{S/M}^i|^3}\right) \tag{40}$$

where $\mu_{_M}$, $\mu_{_E}$, and $\mu_{_S}$ are the gravitational constants for the Moon, Earth, and Sun respectively with $\mathbf{r}_{E/M}^i$ and $\mathbf{r}_{E/S}^i$ representing the position vectors of the Earth and Sun with respect to the Moon in Moon-centered inertial coordinates.

Non-Gravitational Forces and Torques The chaser vehicle's non-gravitational acceleration inputs comprise of the forces due to the onboard actuators $\mathbf{f}_{act}^i$ and the true mass state, $m_c = m_i - m_e$.

$$\mathbf{u}_a^i = \mathbf{g}(\mathbf{x}, \mathbf{f}_{act}^i) = (m_i - m_e)^{-1}\mathbf{f}_{act}^i \tag{41}$$

The non-gravitational torque inputs also include the onboard thruster actuators $\boldsymbol{\tau}_{act}^c$.

$$\mathbf{u}_\tau^c = \mathbf{m}(\boldsymbol{\tau}_{act}^c) = \boldsymbol{\tau}_{act}^c \tag{42}$$

Actuator Thrust The actual inertial forces imparted on a vehicle due to a continuous thrust or finite burn $\mathbf{f}_{act}^i$ is a function of the commanded thrust in the chaser thruster actuator frame $\check{\mathbf{f}}_{act}^a$, the vehicle's attitude $\boldsymbol{\theta}^c$, the thruster bias $\mathbf{b}_{_T}^a$, misalignment $\boldsymbol{\epsilon}_{_T}^a$, scale factor $\mathbf{s}_{_T}^a$, and noise $\boldsymbol{\nu}_{_T}^a$.

$$\mathbf{f}_{act}^i = \mathbf{g}_{act}(\mathbf{x}, \hat{\mathbf{x}}, \boldsymbol{\nu}) = \bar{\mathbf{T}}_c^i\left(\mathbf{I} + [\boldsymbol{\theta}^c\times]\right)\bar{\mathbf{T}}_a^c\left[\left(\mathbf{I} - [\boldsymbol{\epsilon}_{_T}^a\times]\right)\left(\mathbf{I} + [\mathbf{s}_{_T}^a\setminus]\right)\check{\mathbf{f}}_{act}^a + \mathbf{b}_{_T}^a + \boldsymbol{\nu}_{_T}^a\right] \tag{43}$$

The commanded thrust in the thruster actuator frame $\check{\mathbf{f}}_{act}^a$ is a function of the required inertial thrust $\hat{\mathbf{f}}_{act}^i$ and it compensates for the estimated thruster error parameter states.

$$\check{\mathbf{f}}_{act}^a = \left(\mathbf{I} - [\hat{\mathbf{s}}_{_T}^a\setminus]\right)\left(\mathbf{I} + [\hat{\boldsymbol{\epsilon}}_{_T}^a\times]\right)\left[\bar{\mathbf{T}}_c^a\left(\mathbf{I} - [\hat{\boldsymbol{\theta}}^c\times]\right)\bar{\mathbf{T}}_i^c\hat{\mathbf{f}}_{act}^i - \hat{\mathbf{b}}_{_T}^a\right] \tag{44}$$

The required inertial acceleration $\hat{\mathbf{f}}_{act}^i$ can be a constant thrust, the output of a continuous PD flight controller, or derived from an onboard targeting/guidance algorithm.

Open-Loop Thrust Profile For vehicles that have a constant thrust in the body frame or have a particular thrust profile to follow, this can be modeled as an open-loop thrust that is not dependent on the navigation state.

$$\hat{\mathbf{f}}^i_{act} = \hat{\mathbf{g}}_{act}() = \bar{\mathbf{f}}^i_{act}(t) \tag{45}$$

Closed-Loop Controller Thrust To implement a thrust model based on a simple closed-loop PD flight controller (i.e. during the final approach and docking phase), this can be done having a desired relative position and velocity states, $\bar{\mathbf{r}}^i_{rel}$ and $\bar{\mathbf{v}}^i_{rel}$, and determining the difference with the current estimated relative state between the chaser and target spacecraft, $\hat{\mathbf{r}}^i_{rel} = \hat{\mathbf{r}}^i_c - \hat{\mathbf{r}}^i_t$ and $\hat{\mathbf{v}}^i_{rel} = \hat{\mathbf{v}}^i_c - \hat{\mathbf{v}}^i_t$.

$$\hat{\mathbf{f}}^i_{act} = \hat{\mathbf{g}}_{act}(\hat{\mathbf{x}}) = \hat{\mathbf{K}}_r(\bar{\mathbf{r}}^i_{rel} - \hat{\mathbf{r}}^i_{rel}) + \hat{\mathbf{K}}_v(\bar{\mathbf{v}}^i_{rel} - \hat{\mathbf{v}}^i_{rel}) \tag{46}$$

The gains are specified by the natural frequency $\omega_{_T}$ and the damping ratio $\zeta_{_T}$ for the translational control along with the estimated chaser vehicle's mass $\hat{m}_c$.

$$\hat{\mathbf{K}}_r = 2\zeta_{_T}\omega_{_T}\hat{m}_c\,\mathbf{I}_{3\times3} \qquad\qquad \hat{\mathbf{K}}_v = \omega^2_{_T}\hat{m}_c\,\mathbf{I}_{3\times3} \tag{47}$$

Targeting/Guidance Commanded Thrust The command thrust can also come from an onboard targeting and guidance algorithm such as a two-level targeter to execute large orbital finite burns [10–12].

$$\hat{\mathbf{f}}^i_{act} = \hat{\mathbf{g}}_{act}(\hat{\mathbf{x}}) = \hat{\mathbf{g}}_{guid}(\hat{\mathbf{x}}) \tag{48}$$

Actuator Torques The actual torque imparted on the chaser vehicle from onboard thrusters $\boldsymbol{\tau}^c_{act}$ is a function of the commanded torque $\check{\boldsymbol{\tau}}^a_{act}$ and the thruster bias $\mathbf{b}^a_\tau$, misalignment $\boldsymbol{\epsilon}^a_\tau$, scale factor $\mathbf{s}^a_\tau$, and noise terms $\boldsymbol{\nu}^a_\tau$.

$$\boldsymbol{\tau}^c_{act} = \mathbf{m}_{act}(\mathbf{x}, \hat{\mathbf{x}}, \check{\mathbf{y}}^a_{\tilde{\boldsymbol{\omega}}}, \boldsymbol{\nu}) = \bar{\mathbf{T}}^c_a\left[(\mathbf{I} - [\boldsymbol{\epsilon}^a_\tau\times])\,(\mathbf{I} + [\mathbf{s}^a_\tau\backslash])\,\check{\boldsymbol{\tau}}^a_{act} + \mathbf{b}^a_\tau + \boldsymbol{\nu}^a_\tau\right] \tag{49}$$

The commanded torque $\check{\boldsymbol{\tau}}^a_{act}$ compensates for the estimated torque actuator error parameters and the required torque $\hat{\boldsymbol{\tau}}^b_{act}$.

$$\check{\boldsymbol{\tau}}^a_{act} = (\mathbf{I} - [\hat{\mathbf{s}}^a_\tau\backslash])\,(\mathbf{I} + [\hat{\boldsymbol{\epsilon}}^a_\tau\times])\left[\bar{\mathbf{T}}^a_c\hat{\boldsymbol{\tau}}^c_{act} - \hat{\mathbf{b}}^a_\tau\right] \tag{50}$$

The required torque $\hat{\boldsymbol{\tau}}^c_{act}$ is derived from the onboard control system currently modeled as a PD attitude controller where the compensated gyro measurement is used $\check{\mathbf{y}}^c_{\tilde{\boldsymbol{\omega}}}$.

$$\hat{\boldsymbol{\tau}}^c_{act} = \hat{\mathbf{m}}_{act}(\hat{\mathbf{x}}) = \hat{\mathbf{K}}_\theta(\delta\hat{\boldsymbol{\theta}}^c) + \hat{\mathbf{K}}_\omega(\bar{\boldsymbol{\omega}}^c - \check{\mathbf{y}}^c_{\tilde{\boldsymbol{\omega}}}) \tag{51}$$

The chaser attitude error $\delta\hat{\boldsymbol{\theta}}^c$ is the small angle rotation vector between the desired inertial-to-chaser body quaternion $\bar{\mathbf{q}}^b_i$ and the estimated inertial-to-chaser body quaternion $\hat{\mathbf{q}}^i_b$.

$$\left[\frac{1}{2}\delta\hat{\boldsymbol{\theta}}^c\;1\right]^T = \bar{\mathbf{q}}^c_i \otimes \hat{\mathbf{q}}^i_c \tag{52}$$

where the attitude error $\delta\hat{\boldsymbol{\theta}}^c$ is approximately the difference between the required $\bar{\boldsymbol{\theta}}^c$ and estimated small angle rotation vector $\hat{\boldsymbol{\theta}}^c$.

$$\delta\hat{\boldsymbol{\theta}}^c \approx \bar{\boldsymbol{\theta}}^c - \hat{\boldsymbol{\theta}}^c \tag{53}$$

Pointing algorithms that either track the target vehicle or hold a relative orientation of the chaser ultimately determines the desired attitude $\bar{\mathbf{q}}^b_i$. The gains are specified by the natural frequency ω_τ and the damping ratio ζ_τ of the rotational controller along with the vehicle's moments of inertia $\hat{I}$.

$$\hat{\mathbf{K}}_\theta = 2\zeta_\tau\omega_\tau\hat{I} \qquad\qquad \hat{\mathbf{K}}_\omega = \omega^2_\tau\hat{I} \tag{54}$$

Inertial Sensor Models The compensated accelerometer measurement $\check{\mathbf{y}}^i_{\tilde{\mathbf{a}}}$ utilized to propagate the chaser's translational states accounts for the estimated accelerometer error parameters and the transformation of the measurement from the body frame to the inertial frame.

$$\check{\mathbf{y}}^i_{\tilde{\mathbf{a}}} = \mathbf{c}_a(\mathbf{x}, \hat{\mathbf{x}}, \mathbf{u}^i_a, \boldsymbol{\eta}) = \bar{\mathbf{T}}^i_b \left(\mathbf{I} + [\hat{\boldsymbol{\theta}}^c \times]\right) (\mathbf{I} + [\hat{\boldsymbol{\epsilon}}^c_{\tilde{a}} \times]) \left[(\mathbf{I} - [\hat{\mathbf{s}}^c_{\tilde{a}} \backslash]) \, \tilde{\mathbf{y}}^c_{\tilde{\mathbf{a}}} - \hat{\mathbf{b}}^c_{\tilde{a}}\right] \tag{55}$$

The actual accelerometer measurement $\tilde{\mathbf{y}}^c_{\tilde{\mathbf{a}}}$ is a function of the true non-gravitational acceleration, the true accelerometer error parameters, and the accelerometer noise.

$$\tilde{\mathbf{y}}^c_{\tilde{\mathbf{a}}} = (\mathbf{I} + [\mathbf{s}^c_{\tilde{a}} \backslash]) \left[(\mathbf{I} - [\boldsymbol{\epsilon}^c_{\tilde{a}} \times]) (\mathbf{I} - [\boldsymbol{\theta}^c \times]) \, \bar{\mathbf{T}}^b_i \mathbf{u}^i_a + \mathbf{b}^c_{\tilde{a}} + \boldsymbol{\eta}^c_{\tilde{a}}\right] \tag{56}$$

where the non-gravitational acceleration inputs include $\mathbf{u}^i_a = m_c^{-1} \mathbf{f}^i_{act}$.

The compensated gyro measurement $\check{\mathbf{y}}^c_{\tilde{\boldsymbol{\omega}}}$ accounts for the estimated gyro error parameters.

$$\check{\mathbf{y}}^c_{\tilde{\boldsymbol{\omega}}} = \mathbf{c}_\omega(\mathbf{x}, \hat{\mathbf{x}}, \boldsymbol{\eta}) = (\mathbf{I} + [\hat{\boldsymbol{\epsilon}}^c_{\tilde{\omega}} \times]) \left[(\mathbf{I} - [\hat{\mathbf{s}}^c_{\tilde{\omega}} \backslash]) \, \tilde{\mathbf{y}}^c_{\tilde{\boldsymbol{\omega}}} - \hat{\mathbf{b}}^c_{\tilde{\omega}}\right] \tag{57}$$

The actual gyro measurement $\tilde{\mathbf{y}}^c_{\tilde{\boldsymbol{\omega}}}$ is a function of the true angular rate, the true gyro error parameters, and the gyro angular random walk.

$$\tilde{\mathbf{y}}^c_{\tilde{\boldsymbol{\omega}}} = (\mathbf{I} + [\mathbf{s}^c_{\tilde{\omega}} \backslash]) \left[(\mathbf{I} - [\boldsymbol{\epsilon}^c_{\tilde{\omega}} \times]) \, \boldsymbol{\omega}^c + \mathbf{b}^c_{\tilde{\omega}} + \boldsymbol{\eta}^c_{\tilde{\omega}}\right] \tag{58}$$

Grouping the accelerometer and gyro velocity and angular random walk terms $\boldsymbol{\eta} = [\boldsymbol{\eta}^c_{\tilde{a}}; \boldsymbol{\eta}^c_{\tilde{\omega}}]$, the covariance of the continuous measurement noise is given by

$$E[\boldsymbol{\eta}(t)\boldsymbol{\eta}(t)^T] = \mathbf{S}_\eta(t)\delta(t - t') \tag{59}$$

Expelled Propellant Mass Models The mass flow rate from each thruster β_k is a function of the initial chaser vehicle mass m_i, the total expelled propellant mass m_e, the thruster's nominal specific impulse $\bar{I}_{sp_k}$ and its bias b_{Isp_k}, the gravitational constant g, and the thrust acceleration magnitude a_k.

$$\beta_k = b(\mathbf{x}, a_k) = \left[\frac{(m_i - m_e)}{(\bar{I}_{sp_k} + b_{Isp_k}) \cdot g}\right] a_k \tag{60}$$

The acceleration magnitude a_k from a particular thruster is derived from the force produced by the thruster itself $\mathbf{f}^a_k$

$$a_k = |\mathbf{a}^a_k| = |(m_i - m_e)^{-1} \mathbf{f}^a_k| \tag{61}$$

The actual thrust produced by a specific jet depends on the commanded thrust and torques, $\check{\mathbf{f}}^a_{act}$ and $\check{\boldsymbol{\tau}}^a_{act}$, as defined in Eqn 44 and 50 respectively.

$$\mathbf{f}^a_k = \mathbf{g}_k(\check{\mathbf{f}}^a_{act}, \check{\boldsymbol{\tau}}^a_{act}) \tag{62}$$

The utilization of each thruster can be computed using a (6xn) thruster layout matrix, $\bar{\mathbf{A}}_u$, which consists of the nominal or baseline lateral thrusts $\bar{\mathbf{f}}^a_k$ and rotational torques $\bar{\boldsymbol{\tau}}^a_k$ generated if each jet is independently activated.

$$\bar{\mathbf{A}}_u = \begin{bmatrix} \bar{\mathbf{f}}^a_1, & \bar{\mathbf{f}}^a_2, \ ..., & \bar{\mathbf{f}}^a_k, \ ..., & \bar{\mathbf{f}}^a_n \\ \bar{\boldsymbol{\tau}}^a_1, & \bar{\boldsymbol{\tau}}^a_2, \ ..., & \bar{\boldsymbol{\tau}}^a_k, \ ..., & \bar{\boldsymbol{\tau}}^a_n \end{bmatrix} \tag{63}$$

The *throttle level* or scale $\mathbf{t}_u$ is a unit less vector that represents the level of thrust generated for each jet or the amount of time a thruster is active,

$$\mathbf{t}_u = \begin{bmatrix} t_{u_1}; \ t_{u_2}; \ ...; \ t_{u_k}; \ ...; \ t_{u_n} \end{bmatrix} \tag{64}$$

The thruster selection logic, such as a simlex algorithm, determines the *level* for each thruster to achieve the commanded thrust and torques, $\check{\mathbf{u}} = [\check{\mathbf{f}}^a_{act}; \check{\boldsymbol{\tau}}^a_{act}]$, such that

$$\bar{\mathbf{A}}_u \cdot \mathbf{t}_u = \check{\mathbf{u}} \tag{65}$$

Solving for the *throttle level* for each jet,

$$\mathbf{t}_u = (\bar{\mathbf{A}}_u^T \bar{\mathbf{A}})_u^{-1} \bar{\mathbf{A}}_u^T \check{\mathbf{u}} \tag{66}$$

identifies the actual thrust required to produce the commanded thrust and torque

$$\mathbf{f}_k^a = \bar{\mathbf{f}}_k^a \cdot t_{u_k} \tag{67}$$

NRHO RPOD State Update

The potential discrete sensor measurements utilized during RPOD are numerous such as star tracker, ground updates from the deep space network (DSN), relative optical camera bearing measurements, relative S-band ranging, lidar, and an assortment of other potential vision based techniques. Ultimately, a combination of sensor types and quality are examined to determine a sensor suite that will satisfy mission objectives. This section summarizes the fundamental equations to update the augmented state and onboard navigation state covariance matrices when discrete measurements are processed.

Measurements provide information to support the estimation of the current vehicle state, but measurements themselves do not alter the actual physical state of the spacecraft, including the expelled propellant mass. As a result, the true state after a measurement update $\mathbf{x}^+$ equals the true state prior to the measurement update $\mathbf{x}^-$. Similarly, the design state x^+ will also remain unchanged when a discrete measurement is processed. However, the navigation state after a measurement update $\hat{\mathbf{x}}^+$ is altered from its value prior to the measurement $\hat{\mathbf{x}}^-$ based on the difference between the actual measurement $\tilde{\mathbf{z}}$ and its prediction $\hat{\mathbf{z}}$,

$$\mathbf{x}^+ = \mathbf{x}^- \qquad \hat{\mathbf{x}}^+ = \hat{\mathbf{x}}^- + \hat{\mathbf{K}}\left[\tilde{\mathbf{z}} - \hat{\mathbf{z}}\right] \qquad \mathrm{x}^+ = \mathrm{x}^- \tag{68}$$

where $\hat{\mathbf{K}} = \hat{\mathbf{P}}^- \hat{\mathbf{H}}^T \left[\hat{\mathbf{H}} \hat{\mathbf{P}}^- \hat{\mathbf{H}}^T + \hat{\mathbf{R}}\right]^{-1}$ is the onboard Kalman gain. The true measurement $\tilde{\mathbf{z}}$ is a function of the true state $\mathbf{x}^-$ and the actual measurement noise $\boldsymbol{\epsilon}$ where the strength of the discrete measurement noise is $E\left[\boldsymbol{\epsilon}_k \boldsymbol{\epsilon}_{k'}^T\right] = \mathbf{R}\, \delta_{kk'}$. The predicted measurement $\hat{\mathbf{z}}$ is a function of the navigation states. When designing the onboard filter covariance equations, the assumed sensor measurement model $\tilde{\mathrm{z}}$ is a function of the design state x^- and the anticipated sensor noise $\hat{\boldsymbol{\epsilon}}$ where onboard sensor noise assumed $E\left[\hat{\boldsymbol{\epsilon}}_k \hat{\boldsymbol{\epsilon}}_{k'}^T\right] = \hat{\mathbf{R}}\, \delta_{kk'}$

$$\tilde{\mathbf{z}} = \mathbf{h}(\mathbf{x}^-, \boldsymbol{\epsilon}) \qquad \hat{\mathbf{z}} = \hat{\mathbf{h}}(\hat{\mathbf{x}}^-) \qquad \tilde{\mathrm{z}} = \hat{\mathbf{h}}(\mathrm{x}^-, \hat{\boldsymbol{\epsilon}}) \tag{69}$$

NRHO RPOD State Correction

The true, navigation, and design state impulsive dynamics, $\Delta\mathbf{f}$, $\Delta\hat{\mathbf{f}}$, and $\Delta\mathrm{f}$ are a function of the chaser true, navigation, and design states prior to the burn, $\mathbf{x}^{-c}$, $\hat{\mathbf{x}}^{-c}$, and x^{-c}, and the actuator impulsive control input $\Delta\mathbf{u}_a^i$, the detected velocity change $\Delta\check{\mathbf{y}}_{\hat{\mathbf{a}}}^i$, and the design $\Delta\mathrm{u}_a^i$.

$$\mathbf{x}^{+c} = \mathbf{x}^{-c} + \Delta\mathbf{f}(\mathbf{x}^{-c}, \Delta\mathbf{u}_a^i) \qquad \hat{\mathbf{x}}^{+c} = \hat{\mathbf{x}}^{-c} + \Delta\hat{\mathbf{f}}(\hat{\mathbf{x}}^{-c}, \Delta\check{\mathbf{y}}_{\hat{\mathbf{a}}}^i) \qquad \mathrm{x}^{+c} = \mathrm{x}^{-c} + \Delta\mathrm{f}(\mathrm{x}^{-c}, \Delta\mathrm{u}_a^i) \tag{70}$$

As summarized in Table 2, the two states impacted by the impulsive correction are the chaser vehicle's velocity state $\mathbf{v}_c^i$ and the total propellant expelled mass state m_e.

Impulsive State Correction The impulsive state correction control input $\Delta\mathbf{u}_a^i$ is a function of the true and navigation state prior to the burn, $\mathbf{x}^{-c}$ and $\hat{\mathbf{x}}^{-c}$, and the impulsive thruster noise $\boldsymbol{\nu}$. For now, it only consists of the actual translational delta-v imparted on the chaser vehicle $\Delta\mathbf{v}^i$ due to an impulsive actuation which is a function of the commanded delta-v in the thruster actuator frame $\Delta\check{\mathbf{v}}^a$, the vehicle's attitude $\boldsymbol{\theta}^c$, the thruster bias $\mathbf{b}_{\Delta v}^a$, misalignment $\boldsymbol{\epsilon}_{\Delta v}^a$, scale factor $\mathbf{s}_{\Delta v}^a$, and noise $\boldsymbol{\nu}_{\Delta v}^a$ as introduced previously in Eqn 25.

$$\Delta\mathbf{u}_a^i = \Delta\mathbf{g}(\mathbf{x}^{-c}, \hat{\mathbf{x}}^{-c}, \boldsymbol{\nu}) = \Delta\mathbf{v}^i = \bar{\mathbf{T}}_c^i \left(\mathbf{I} + [\boldsymbol{\theta}^c\times]\right) \bar{\mathbf{T}}_a^c \left[\left(\mathbf{I} - [\boldsymbol{\epsilon}_{\Delta v}^a\times] + \mathbf{I}s_{\Delta v}^a\right) \Delta\check{\mathbf{v}}^a + \mathbf{b}_{\Delta v}^a + \boldsymbol{\nu}_{\Delta v}^a\right] \tag{71}$$

True (Environment) States	Navigation States	Design States
$\left[\mathbf{v}_c^i\right]^{+c} = \left[\mathbf{v}_c^i\right]^{-c} + \Delta\mathbf{u}_a^i$	$\left[\hat{\mathbf{v}}_c^i\right]^{+c} = \left[\hat{\mathbf{v}}_c^i\right]^{-c} + \Delta\check{\mathbf{y}}_{\tilde{\mathbf{a}}}^i$	$\left[\mathrm{v}_c^i\right]^{+c} = \left[\mathrm{v}_c^i\right]^{-c} + \Delta\mathrm{u}_a^i$
$[m_e]^{+c} = [m_e]^{-c} + \sum_{k=1}^{n} \Delta m_{e_k}$	$[\hat{m}_e]^{+c} = [\hat{m}_e]^{-c} + \sum_{k=1}^{n} \Delta\hat{m}_{e_k}$	$[\mathrm{m}_e]^{+c} = [\mathrm{m}_e]^{-c} + \sum_{k=1}^{n} \Delta m_{e_k}$
$\mathbf{x}^{+c} = \mathbf{x}^{-c} + \Delta\mathbf{f}(\mathbf{x}^{-c}, \Delta\mathbf{u}_a^i)$	$\hat{\mathbf{x}}^{+c} = \hat{\mathbf{x}}^{-c} + \Delta\hat{\mathbf{f}}(\hat{\mathbf{x}}^{-c}, \Delta\check{\mathbf{y}}_{\tilde{\mathbf{a}}}^i)$	$\mathrm{x}^{+c} = \mathrm{x}^{-c} + \Delta\hat{\mathbf{f}}(\mathrm{x}^{-c}, \Delta\mathrm{u}_a^i)$

Table 2. True and Navigation Impulsive State Dynamics

The commanded delta-v in the thruster actuator frame $\Delta\check{\mathbf{v}}^a$ is a function of the required inertial delta-v $\Delta\bar{\mathbf{v}}^i$ and it compensates for the estimated thruster error parameter states.

$$\Delta\check{\mathbf{v}}^a = \left(\mathbf{I} + [\hat{\boldsymbol{\epsilon}}_{\Delta v}^a\times] - \mathbf{I}\hat{s}_{\Delta v}^a\right)\left[\bar{\mathbf{T}}_c^a\left(\mathbf{I} - [\hat{\boldsymbol{\theta}}^c\times]\right)\bar{\mathbf{T}}_i^c\Delta\bar{\mathbf{v}}^i - \hat{\mathbf{b}}_{\Delta v}^a\right] \tag{72}$$

The required delta-v, $\Delta\bar{\mathbf{v}}^i$, for the relative rendezvous burns is generated using the linearized relative targeting algorithm, which is similar to CW-targeting but modified for NRHO relative motion dynamics,

$$\Delta\bar{\mathbf{v}}^i = \Delta\hat{\mathbf{g}}(\hat{\mathbf{x}}) = \hat{\mathbf{T}}_{rel}^i\left[\boldsymbol{\Phi}_{rv}^{-1}\left(\bar{\mathbf{r}}^{rel} - \boldsymbol{\Phi}_{rr}\hat{\mathbf{r}}^{rel}\right) - \hat{\mathbf{v}}^{rel}\right] \tag{73}$$

where $\hat{\mathbf{T}}_{rel}^i$ is the inertial-to-relative transformation matrix and the estimated relative position and velocity vectors are derived from the chaser and target inertial position and velocity vectors, $\hat{\mathbf{r}}^{rel} = \hat{\mathbf{T}}_i^{rel}(\hat{\mathbf{r}}_c^i - \hat{\mathbf{r}}_t^i)$ and $\hat{\mathbf{v}}^{rel} = \hat{\mathbf{T}}_i^{rel}(\hat{\mathbf{v}}_c^i - \hat{\mathbf{v}}_t^i)$.

Impulsive Inertial Measurement The compensated *instantaneous* accelerometer measurement in the inertial frame used to *correct* the chaser velocity states accounts for the estimated accelerometer error parameters and the duration of the actuator burn, Δt_a.

$$\Delta\check{\mathbf{y}}_{\tilde{\mathbf{a}}}^i = \Delta\mathbf{c}_a(\mathbf{x}^{-c}, \hat{\mathbf{x}}^{-c}, \Delta\mathbf{u}_a^i, \boldsymbol{\eta}) = \bar{\mathbf{T}}_b^i\left(\mathbf{I} + [\hat{\boldsymbol{\theta}}^c\times]\right)(\mathbf{I} + [\hat{\boldsymbol{\epsilon}}_{\tilde{a}}^c\times])\left[(\mathbf{I} - [\hat{\mathbf{s}}_{\tilde{a}}^c\backslash])\,\Delta\tilde{\mathbf{y}}_{\tilde{\mathbf{a}}}^c - \hat{\mathbf{b}}_{\tilde{a}}^c\Delta t_a\right] \tag{74}$$

The actual accelerometer measurement $\Delta\tilde{\mathbf{y}}_{\tilde{\mathbf{a}}}^c$ is a function of the true impulsive burn, the true accelerometer error parameters, the accelerometer noise, and thuster on-time.

$$\Delta\tilde{\mathbf{y}}_{\tilde{\mathbf{a}}}^c = (\mathbf{I} + [\mathbf{s}_{\tilde{a}}^c\backslash])\left[(\mathbf{I} - [\boldsymbol{\epsilon}_{\tilde{a}}^c\times])\,(\mathbf{I} - [\boldsymbol{\theta}^c\times])\,\bar{\mathbf{T}}_i^c\Delta\mathbf{u}_a^i + \mathbf{b}_{\tilde{a}}^c\Delta t_a + \boldsymbol{\eta}_{\tilde{a}}^c\sqrt{\Delta t_a}\right] \tag{75}$$

The thruster on-time is determined by the mass, magnitude of the delta-v burn $|\Delta\mathbf{v}^i|$ derived in Eqn 71, and the force of the thruster f_a.

$$\Delta t_a = \left[\frac{(m_i - m_e)}{f_a}\right]|\Delta\mathbf{v}^i| \tag{76}$$

Impulsive Expelled Propellant Mass The expelled propellant mass during an impulsive translational burn or translational maneuver is derived from the rocket equation referenced previously in Eqn 2

$$\Delta m_{e_k} = \Delta b(\mathbf{x}^{-c}, \Delta v_k) = (m_i - m_e^{-c})\left[1 - e^{-\left(\frac{\Delta v_k}{I_{sp}\cdot g}\right)}\right] \tag{77}$$

The delta-v magnitude Δv_k from a particular thruster equals the delta-v produced by the jet in the actuator frame,

$$\Delta v_k = |\Delta\mathbf{v}_k^a| \tag{78}$$

which depends on the commanded delta-v $\Delta\check{\mathbf{v}}^a$ as defined in Eqn 72

$$\Delta\mathbf{v}_k^a = \Delta\mathbf{g}_k(\Delta\check{\mathbf{v}}^a) \tag{79}$$

The utilization of each impulsive thruster can be computed using a (6xn) thruster layout matrix, $\bar{\mathbf{A}}_{\Delta u}$, which consists of the nominal or baseline translational delta-v $\Delta\bar{\mathbf{v}}_k^a$ and rotational instantaneous angular-rates $\Delta\bar{\boldsymbol{\omega}}_k^a$ generated if each jet is independently activated.

$$\bar{\mathbf{A}}_{\Delta u} = \begin{bmatrix} \Delta\bar{\mathbf{v}}_1^a, & \Delta\bar{\mathbf{v}}_2^a, \ ..., & \Delta\bar{\mathbf{v}}_k^a, \ ..., & \Delta\bar{\mathbf{v}}_n^a \\ \Delta\bar{\boldsymbol{\omega}}_1^a, & \Delta\bar{\boldsymbol{\omega}}_2^a, \ ..., & \Delta\bar{\boldsymbol{\omega}}_k^a, \ ..., & \Delta\bar{\boldsymbol{\omega}}_n^a \end{bmatrix} \tag{80}$$

The *throttle level* or scale $\mathbf{t}_u$ is a unit less vector that represents the level of delta-v generated for each jet,

$$\mathbf{t}_{\Delta u} = \left[t_{\Delta u_1};\ t_{\Delta u_2};\ ...;\ t_{\Delta u_k};\ ...;\ t_{\Delta u_n}\right] \tag{81}$$

The thruster selection logic, such as a simlex algorithm, determines the *level* for each thruster to achieve the commanded thrust and torques, $\Delta\check{\mathbf{u}} = [\Delta\check{\mathbf{v}}^a; \mathbf{0}]$, such that

$$\bar{\mathbf{A}}_{\Delta u} \cdot \mathbf{t}_{\Delta u} = \Delta\check{\mathbf{u}} \tag{82}$$

Solving for the impulsive *throttle level* for each jet,

$$\mathbf{t}_{\Delta u} = (\bar{\mathbf{A}}_{\Delta u}^T \bar{\mathbf{A}})_{\Delta u}^{-1} \bar{\mathbf{A}}_{\Delta u}^T \Delta\check{\mathbf{u}} \tag{83}$$

identifies the actual thrust required to produce the commanded thrust and torque

$$\Delta\mathbf{v}_k^a = \Delta\bar{\mathbf{v}}_k^a \cdot t_{\Delta u_k} \tag{84}$$

DELTA-V DISPERSION MODELING

Given the overview of the different thruster models and the theoretical foundation of implementing them in a linear covariance simulation framework for an NRHO RPOD scenario, this section presents the different techniques for computing the actual delta-v dispersions or the propellant dispersions given uncertainty in the GN&C system. These options include and are referenced as 1) Delta-v Magnitude, 2) Delta-v Sum, 3) Delta-v Numerical, and 4) Delta-v Expelled Mass. Depending on the thruster model adopted (impulsive or finite burns, single or multiple thrusters, translational only or translational and rotational), the techniques for computing delta-v and the expected propellant usage is constrained. Below in Table 3 is a summary of the different delta-v dispersion models that can be used in context of the thruster model assumed for the analysis. The delta-v dispersion modeling option that can apply to all the different thruster model configurations is the expelled mass state. If the thruster model assumes only a single and impulsive jet that impacts the translational dynamics only, then all the delta-v dispersion modeling options can be utilized.

IMPULSIVE	Trans Only	Trans/Rot
Single Thruster	All	Mass
Multiple Thrusters	Mass	Mass

FINITE	Trans Only	Trans/Rot
Single Thruster	Mass	Mass
Multiple Thrusters	Mass	Mass

Table 3. Thruster Model Configurations and Delta-v Dispersion Modeling Options

Similar to producing trajectory dispersions and navigation errors, a linear covariance tool can also generate the delta-v dispersions. As introduced in Eqn 71, the executed burn is a function of the current augmented state $\mathbf{X}$ which consists of the true state and navigation state as defined in Eqn 14, $\mathbf{X}^{\mathrm{T}} = [\mathbf{x}^{\mathrm{T}}\ \hat{\mathbf{x}}^{\mathrm{T}}]$.

$$\Delta\mathbf{v}^i = \Delta\mathbf{g}(\mathbf{X}^{-c}, \boldsymbol{\nu})$$

To first order, the perturbation in the delta-v vector from the nominal, $\delta\Delta\mathbf{v}^i = \Delta\mathbf{v}^i - \Delta\bar{\mathbf{v}}^i$, can be expressed as a function of the perturbation in the augmented state $\delta\mathbf{X}$ and burn execution noise $\boldsymbol{\eta}$,

$$\delta\Delta\mathbf{v}^i = \Delta\mathbf{G}_X\delta\mathbf{X} + \Delta\mathbf{G}_\nu\boldsymbol{\nu} \tag{85}$$

where $\Delta\mathbf{G}_X = \frac{\partial\Delta\mathbf{g}(\mathbf{X}^{-c},\boldsymbol{\nu})}{\partial\mathbf{X}}$ and $\Delta\mathbf{G}_\nu = \frac{\partial\Delta\mathbf{g}(\mathbf{X}^{-c},\boldsymbol{\nu})}{\partial\boldsymbol{\nu}}$. By definition, the covariance matrix of the delta-v dispersions is,

$$\mathbf{D}_{\Delta v} = E\left[(\delta\Delta\mathbf{v}^i)(\delta\Delta\mathbf{v}^i)^T\right] \tag{86}$$

Substituting the expression for $\delta\Delta\mathbf{v}$ in Eqn 85 into Eqn 86, the delta-v dispersions covariance $\mathbf{D}_{\Delta v}$ can be expressed in terms of the impulsive thruster noise, $\mathbf{V} = E\left[\boldsymbol{\nu}\boldsymbol{\nu}^T\right]$, and the augmented state covariance matrix, $\mathbf{C} = E\left[\delta\mathbf{X}\delta\mathbf{X}^{\mathrm{T}}\right]$, as defined in Eqn 14.

$$\mathbf{D}_{\Delta v} = \Delta\mathbf{G}_X\mathbf{C}\Delta\mathbf{G}_X^T + \Delta\mathbf{G}_\nu\mathbf{V}\Delta\mathbf{G}_\nu^T \tag{87}$$

Delta-v Magnitude A simple analytical approach to compute the uncertainty of the magnitude of the delta-v originates with the fundamental definition of the magnitude of the burn $|\Delta\mathbf{v}|$ as utilized in the rocket equation

$$|\Delta\mathbf{v}| = \left[(\Delta\mathbf{v}^T)(\Delta\mathbf{v})\right]^{0.5} \tag{88}$$

The perturbation of the magnitude of the delta-v vector due to the perturbation in the augmented states (or delta-v vector) can be derived using the chain rule

$$\delta|\Delta\mathbf{v}| = \left(\frac{\partial|\Delta\mathbf{v}|}{\partial\Delta\mathbf{v}}\right)\delta\Delta\mathbf{v} \tag{89}$$

where $\frac{\partial|\Delta\mathbf{v}|}{\partial\Delta\mathbf{v}} = \mathbf{i}_{\Delta v}^T$ is the transpose of the nominal delta-v unit vector. By definition, the covariance of the perturbation $\mathbf{D}_{|\Delta v|}$ in the magnitude of the maneuver equals

$$\mathbf{D}_{|\Delta v|} = E\left[(\delta|\Delta\mathbf{v}|)(\delta|\Delta\mathbf{v}|)^T\right] = \mathbf{i}_{\Delta v}^T E\left[(\delta\Delta\mathbf{v})(\delta\Delta\mathbf{v})^T\right]\mathbf{i}_{\Delta v} \tag{90}$$

Substituting Eqn 86 into Eqn 90, the covariance of the perturbation $\mathbf{D}_{|\Delta v|}$ in the magnitude of the burn becomes

$$\mathbf{D}_{|\Delta v|} = \mathbf{i}_{\Delta v}^T\mathbf{D}_{\Delta v}\mathbf{i}_{\Delta v} \tag{91}$$

This approach is valid for cases when the nominal delta-v is much larger than the delta-v dispersions. However, for trajectory correction burns when the nominal delta-v is zero, the delta-v unit vector is undefined and this approach breaks down.

Delta-v Sum A simple analytical approach to characterize the variance of the magnitude of the delta-v vector is to take the sum of the variance associated with each component.

$$\mathbf{D}_{|\Delta v|} = \sum_{k=1}^{3}\mathbf{D}_{\Delta v}(k,k) \tag{92}$$

Not only can this approach work for scenarios where the nominal delta-v is small or near zero, this method also seems to be a common and accepted strategy. It represents a conservative upper bound.*

*A variation of this approach is to do the following where the square of the sum is utilized, which can be even more conservative, particularly for burns that may be done with RCS jets

$$\mathbf{D}_{|\Delta v|} = \left(\sum_{k=1}^{3}\sqrt{\mathbf{D}_{\Delta v}(k,k)}\right)^2 \tag{93}$$

Delta-v Numerical Instead of deriving the variance of the delta-v magnitude analytically, the statistics can be computed numerically using the derived delta-v covariance matrix $\mathbf{D}_{\Delta v}$. As illustrated in Figure 5, n sample vectors $\Delta\mathbf{v}_j$ are extracted from the distribution characterizing the delta-v dispersions. Then, for each sample the nominal delta-v vector is added to form a sample of a *true* delta-v burn. The magnitude of each of these resulting vectors is computed. From this collection of delta-v magnitudes, the mean and standard deviation are numerically calculated (along with other delta-v performance metrics such as delta-v 99 percentile).

$$\boldsymbol{\mu}_{|\Delta v|} = \frac{1}{n}\sum_{j=1}^{n}|\Delta\mathbf{v}_j| \qquad \mathbf{D}_{|\Delta v|} = \frac{1}{n-1}\sum_{j=1}^{n}\left(|\Delta\mathbf{v}_j| - \mu_{|\Delta v|}\right)^2 \tag{94}$$

Based on previous experience, this approach has provided the most accurate predictions for rendezvous and close-proximity delta-v estimations. Although this is currently the more trusted solution, this technique does not account for correlations between maneuvers. There is also additional computational resources expended with sampling* which can become a deterring factor when large number of burns are executed.

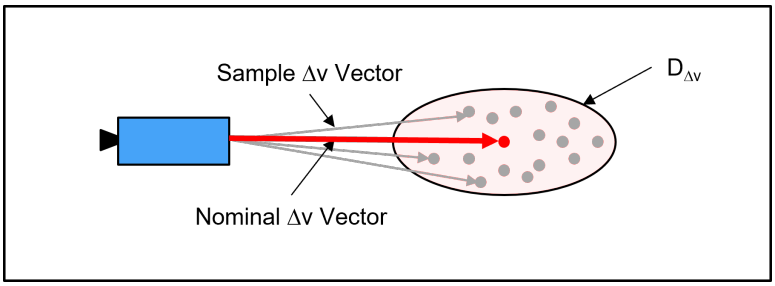


Figure 5. Delta-v Numerical Approach

Delta-v Expelled Mass For many rendezvous burn sequences, such as orbit raising burns, there is a correlation between burns. If the initial orbit raising burn is too large and additional orbital energy has been added, then subsequent burns do not need to be as large. One analytical approach for deriving the uncertainty of the delta-v magnitude that captures the correlation between burns is to include the delta-v magnitude as a state in the augmented state. This is often referred to as adding a *mass state* introduced by Rose [2] to support linear covariance analysis. Although this strategy has the potential to capture the correlation between maneuvers, it is still limited to the previous shortcoming common to most analytical approaches when the nominal delta-v is near zero or the linearization assumptions in computing the delta-v magnitude are violated. This approach has the most broad applications, and in some situations the only option, when considering the different thruster model configurations such as finite burns.

In Eqn 1, the rocket equation connecting the delta-v magnitude and the impulsive expelled mass was summarized.

$$|\Delta\mathbf{v}| = (I_{sp}\cdot g)\ln\left[\frac{(m_i - m_e)}{(m_i - m_e) - \Delta m_e}\right] \tag{95}$$

The variation in the delta-v magnitude to the variation in the expelled mass is

$$\mathbf{G}_{m_e} = \frac{\partial|\Delta\mathbf{v}|}{\partial\Delta m_e} = \frac{(I_{sp}\cdot g)}{(m_i - m_e) - \Delta m_e} \tag{96}$$

such that

$$\delta|\Delta\mathbf{v}| = \mathbf{G}_{m_e}\delta\Delta m_e \tag{97}$$

*Alternate solutions have been generated to support trajectory correction burns without having to sample the statistics for each burn [13].

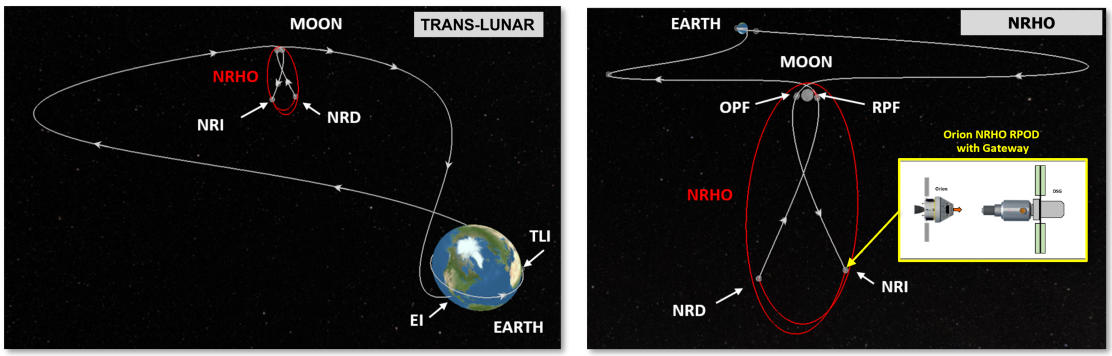
and

$$\mathbf{D}_{|\Delta v|} = \mathbf{G}_{m_e} \mathbf{C}_{m_e} \mathbf{G}_{m_e}^T \tag{98}$$

where $\mathbf{C}_{m_e}$ is the augmented state element associated with the expelled mass state dispersions.

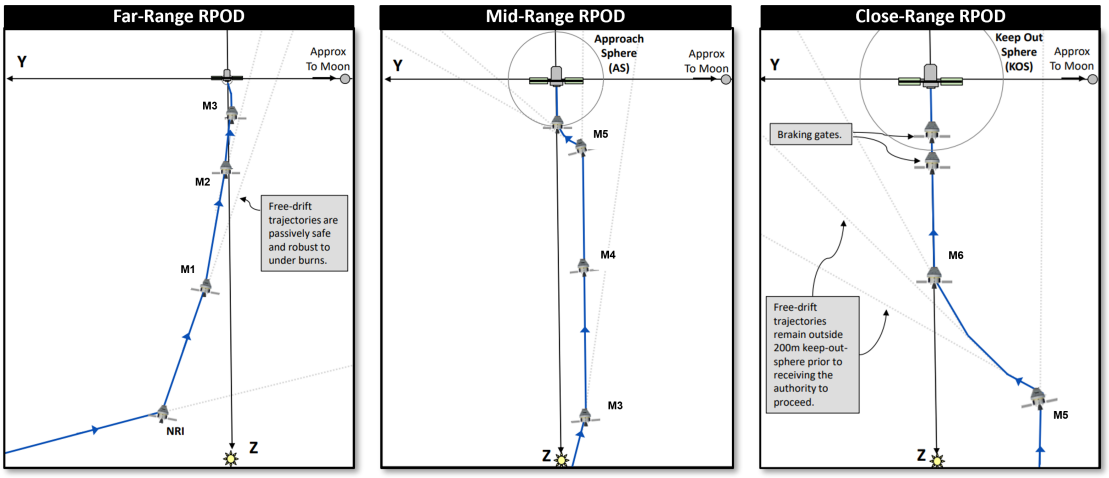
NRHO RENDEZVOUS AND DOCKING CONCEPT OF OPERATIONS

To exercise the development of the different delta-v dispersion models and the influence the various thruster configurations has on computing this performance metric, a rendezvous and docking scenario in a Near Rectlinear Halo Orbit (NRHO) is adopted that is comparable to the NASA Artemis III mission where Orion plans to rendezvous and dock with the Human Landing System (HLS) vehicle. Figure 6 illustrates the location of the NRHO rendezvous profile in the Earth/Moon rotating frame. The view from the Earth to the Moon is shown in Figure 6(a) and an emphasis of the location of the rendezvous and docking at the NRHO insertion (NRI) point is highlighted in Figure 6(b). Following the NRI, a series of far-range, mid-range, and close-range burns are nominally performed until contact as shown in the Sun-referenced LVLH frame in Figure 6(c), Figure 6(d), and Figure 6(e) respectively. For demonstration purposes, the rendezvous scenario will begin at a location in the *close-range* RPOD phase just prior to M5. During this final phase prior to contact, the burns are smaller and are executed with RCS jets while Orion continuously tracks the target vehicle.



(a) Earth-to-Moon View of NRHO RPOD

(b) Moon-to-Earth View of NRHO RPOD



(c) Far-Range NRHO RPOD

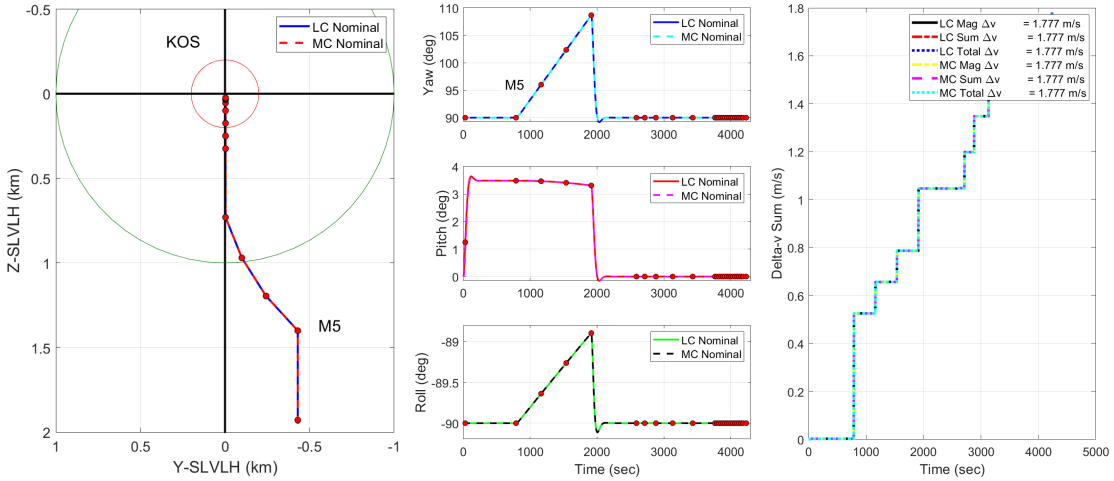
(d) Mid-Range NRHO RPOD

(e) Close-Range NRHO RPOD

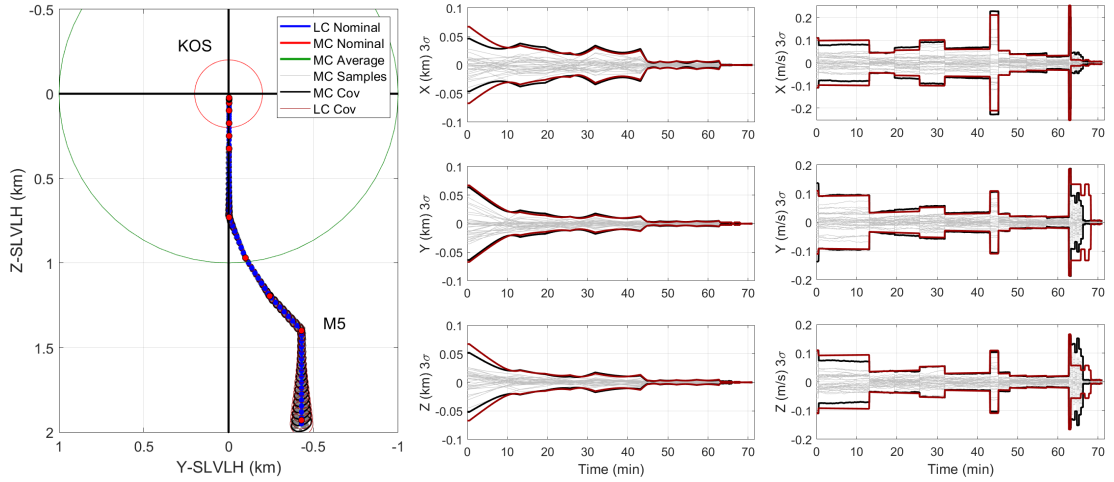
Figure 6. The Orion Artemis III trajectory in a southern Near Rectilinear Halo Orbit (NRHO).

NRHO RENDEZVOUS AND DOCKING PERFORMANCE

The nominal reference trajectory generated in both the LinCov and Monte Carlo tool sets are provided in Figure 7(a) where the solid (blue) line represents the output from the LinCov simulation and the dashed (red) line is the nominal profile generated by the Monte Carlo process. Similarly, the nominal attitude profile simulated in both tool sets in shown in Figure 7(b) and the nominal delta-v values are in Figure 7(c) for the different thruster models (magnitude, sum, mass). The resulting trajectory dispersions, relative position dispersions, and relative velocity dispersions are provided in Figures 7(d), Figure 7(e), and Figure 7(f) where the solid maroon ellipse are the 3-sigma bounds, the solid black ellipse are the 3-sigma sample Monte Carlo results, and the gray lines represent the individual Monte Carlo sample trial runs.



(a) Nominal Close-Range Trajectory (b) Nominal Attitude Profile (c) Nominal Delta-v

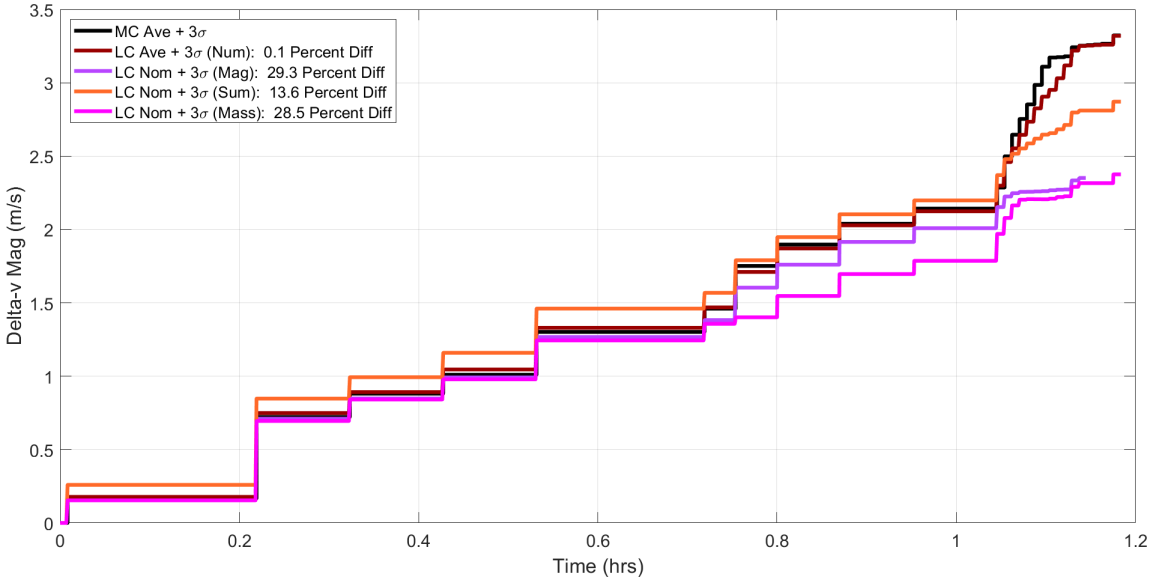


(d) Close-Range Trajectory Dispersions (e) Relative Position Dispersions (f) Relative Velocity Dispersions

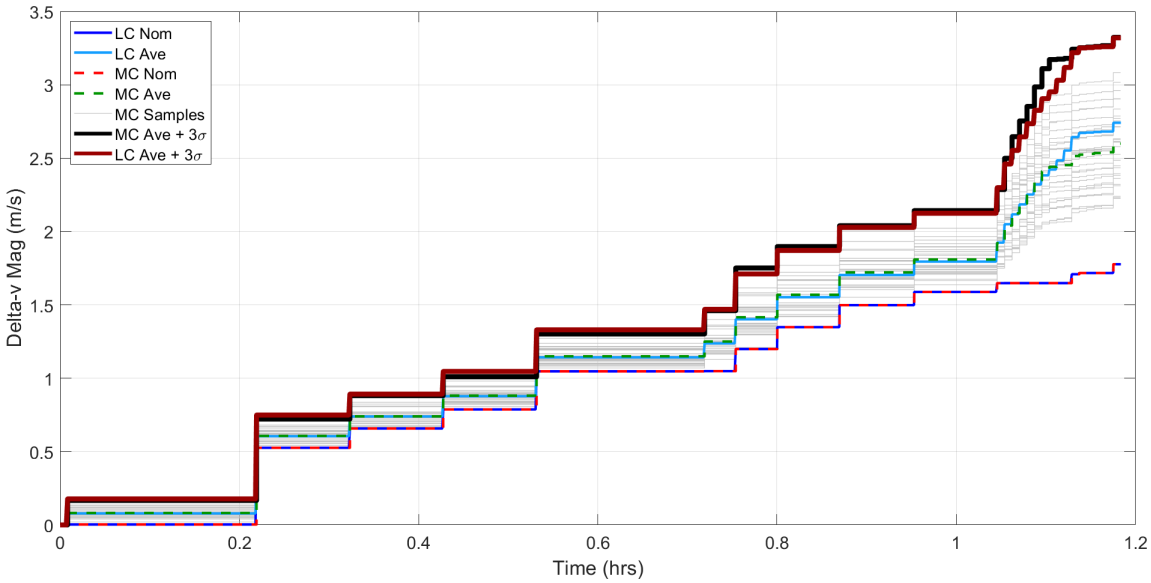
Figure 7. NRHO rendezvous and docking performance results

For a thruster configuration where a single jet is assumed with impulsive burns and translational control only, the resulting delta-v performance statistics using the delta-v dispersion model of 1) Delta-v Magnitude, 2) Delta-v Sum, 3) Delta-v Mass, and 4) Delta-v numerical are captured in Figure 8. Figure 8(a) summarizes the projected total delta-v predictions (nominal or average delta-v plus the 3-sigma dispersions) for each technique and the results are compared to the Monte Carlo outputs. For example, using the numerical ap-

proach, the LinCov results are within 0.1 percent of the final Monte Carlo results for total delta-v. The other approaches differ from 10-30% primarily due to the difference between the mean and nominal values, not the calculation of the predicted 3-sigma delta-v dispersions. Details related to this case are emphasized in Figure 8(b) where the Lincov and Monte Carlo nominal delta-v, average delta-v, and total delta-v are compared for the case when using the numerical approach for extracting the delta-v dispersions.



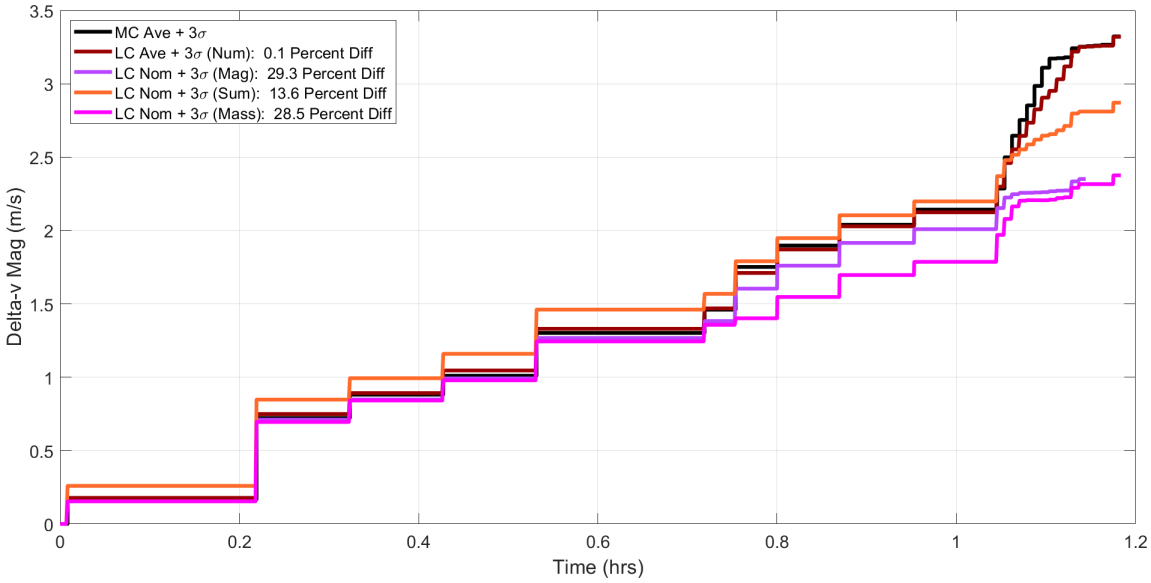
(a) Delta-v Dispersion Summary



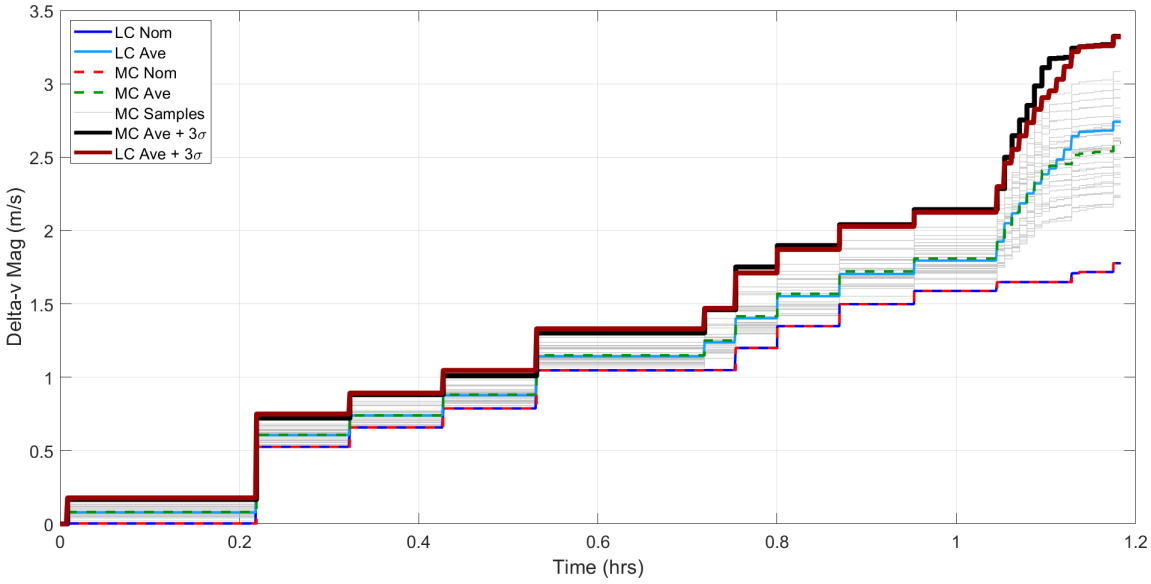
(b) Delta-v Dispersion Numerical

Figure 8. Delta-v Dispersions for a Single, Impulsive, Translational Only Thruster Model

Expanding the thruster model to include multiple jets are provided in Figure 9.



(a) Delta-v Dispersion Summary



(b) Delta-v Dispersion Numerical

Figure 9. Delta-v Dispersions for Multiple, Impulsive, Translational and Rotational Thruster Model

CONCLUSION

The ability to quickly and reliably extract the expected total delta-v or anticipated propellant usage for a mission is a coveted capability enabling the evaluation of the performance metric that some refer to as the currency of space flight. Typically extensive resources are required to identify the propellant budget, particularly when uncertainty in the system such as launch vehicle orbit insertion dispersions, disturbance accelerations acting on the spacecraft, navigation and targeting system errors, and thruster layout design and jet selection logic are considered. The traditional analysis technique to solve this complex problem has been the utilization of Monte Carlo simulation tools where hundreds and thousands of perturbed sample

cases are evaluated using sophisticated models capturing the flight software algorithms, flight hardware, and other critical system operations. A byproduct of this approach yields reliable results, but the time it takes to create and validate the models and then actually process them causes this analysis cycle to be tedious and cumbersomely slow.

Over the past several decades, linear covariance analysis techniques have shown tremendous potential to reliably generate trajectory dispersions and navigation errors in only a fraction of the time. Despite the extensive development and space flight applications, there is still an underlying and justifiable sense of skepticism regarding the ability to reliably predict total delta-v. The purpose of this paper was to address these concerns and doubts by outlining the fundamental linear covariance equations used to compute the delta-v dispersions, give an overview of the different techniques available for calculating this metric, and then compare the results using LinCov to Monte Carlo data. Each of these objectives was accomplished in context of an NRHO rendezvous scenario, anticipated for upcoming NASA Artemis missions. In fact, it was shown that the total delta-v generated by LinCov and Monte Carlo could differ by less than 0.1% for cases using a single, impulsive thruster for translational control only. When jet selection logic is used for multiple thrusters for both translational and rotational control, the two techniques differed by only x.x %.

REFERENCES

[1] A. A. Blagonravov, "Collected works of k. e. tsiokovskity: Volume ii - reactive flying machines," Tech. Rep. NASA TT F-237, National Aeronautics and Space Administration, 1954.

[2] M. B. Rose and D. K. Geller, "Linear covariance techniques for powered ascent," in *AIAA 2010-8175*, 2010.

[3] P. S. Maybeck, *Stochastic models, estimation, and control*, vol. 1. New York: Academic Press, 1979.

[4] D. K. Geller, "Linear covariance techniques for orbital rendezvous analysis and autonomous onboard mission planning," *Journal of Guidance, Control, and Dynamics*, vol. 29, pp. 1404–1414, November-December 2006.

[5] T. J. Moesser and D. K. Geller, "Guidance and navigation linear covariance analysis for lunar powered descent," in *AAS/AIAA Astrodynamics Specialist Conference*, (Mackinac Island, Michigan), AAS 07-313, 19-23 August 2007.

[6] D. Geller and D. Christensen, "Linear Covariance Analysis for Powered Lunar Descent and Landing," *The Journal of Spacecraft and Rockets*, vol. 46, pp. 1231–1248, Nov-Dec 2009.

[7] D. Woffinden, S. Robinson, J. Williams, and Z. Putnam, "Linear covariance analysis techniques to generate navigation and sensor requirements for the safe and precise landing - integrated capabilities evolution (splice) project," in *AIAA Scitech 2019 Forum*, (San Diego, CA), AIAA 2019-0662, 7-11 January 2019 2019.

[8] J. W. Williams, W. E. Brandenburg, D. C. Woffinden, and Z. R. Putnam, "Validation of linear covariance techniques for mars entry, descent, and landing guidance and navigaiton performance analysis," in *AIAA Scitech 2022 Forum*, 2022.

[9] C. R. Gates, "A simplified model of midcourse maneuver execution errors," Tech. Rep. Technical Report No. 32-504, NASA Jet Propulsion Laboratory, California Institute of Technology, 15 October 1963.

[10] B. G. Marchand, M. W. Weeks, C. W. Smith, and S. Scarritt, "Onboard autonoous targeting for the trans-earth phase of orion," *Journal of Guidance, Control, and Dynamics*, vol. 33, pp. 943–956, May-June 2010.

[11] S. Scarritt, B. G. Marchand, A. J. Brown, W. H. Tracy, and M. W. Weeks, "Finite-burn linear targeting algorithm for autonomous path planning guidance," *Journal of Guidance, Control, and Dynamics*, vol. 35, pp. 1605–1615, September-October 2012.

[12] S. K. Scarritt, T. Fill, and S. Robinson, "Advances in orion's on-orbit guidance and targeting system architecture," (Breckenridge, CO), AAS 15-096, 1 Feb - 6 Feb 2015.

[13] Q. Moon and D. Geller, "Regression techniques for the statistics of correction maneuvers magnitudes," (Breckenridge, CO), AAS Guidance and Control Conference, AAS-24-026, 1 Feb - 7 Feb 2024.